NUCLEAR ENERGY LEVELS IN Tm^{169} AND Lu^{175}

Thesis by

Eastman Nibley Hatch

In Partial Fulfillment of the Requirements

for the Degree of

Doctor of Philosophy

California Institute of Technology

Pasadena, California

1956

ACKNOWLEDGMENTS

The investigations reported in this thesis were performed in a research group under the supervision of Professor Jesse W. M. DuMond, and it is the author's pleasure to acknowledge Professor DuMond's interest and guidance. To the other members of the group, each of whom has been helpful, the author wishes to express his thanks.

The patient guidance, the advice and encouragement given by Dr. Pierre Marmier and Dr. Felix Boehm throughout the experiments are deeply appreciated.

This work was supported by the U.S. Atomic Energy Commission.

ABSTRACT

The electron-capture decay of Yb^{169} to Tm^{169} and the beta-decay of Yb^{175} to Lu^{175} have been studied using the curved-crystal gamma-ray diffraction spectrometer, the ring-focusing beta-ray spectrometer, and the semicircular homogeneous-field beta-ray spectrometer. The precision energies and the multipolarities of Tm^{169} and Lu^{175} nuclear transitions have been determined, and energies, spins and parities of the nuclear levels are proposed. The principal experimental techniques are reviewed, and the results of preliminary measurements of the curved-crystal spectrometer reflection coefficient are indicated. The observed nuclear levels and transitions in Tm^{169} and Lu^{175} are discussed on the basis of the Bohr-Mottelson unified nuclear model.

TABLE OF CONTENTS

APPENDICES

LIST OF TABLES

LIST OF FIGURES

PART I

INTRODUCTION

INTRODUCTION

Interest in the study of nuclear spectra of heavy nuclei has been greatly stimulated by recent advances in nuclear theory. In particular, the Bohr-Mottelson unified model (1)(2) has made possible predictions concerning the spectra of nuclei in regions removed from closed shells. With the theoretical prediction of the relative energy spacings of some of the excited states of these nuclei, the determination and precise energy measurement of these excited levels has become increasingly interesting.

For isotopes lying in the regions $155 < A < 185$ and $A > 225$, which are removed from closed shells, the nuclei show large deformations from spherical symmetry (2). According to the Bohr-Mottelson unified model, for axially symmetric nuclei the component of the total nuclear spin I along the symmetry axis is quantized, the quantum number being denoted by K. K actually is a good quantum number only in the limit of extreme deformations. For intermediate deformations K is only approximately a good quantum number.

For odd A nuclei, rotational bands based on intrinsic particle levels are composed of states having the same parity as the intrinsic level and having spins $I = K, K + 1, K + 2, \ldots$ The energy spacing of these levels is given by the expression

$$E_{rot} = \frac{\hbar^2}{2\mathcal{I}} \left\{ I(I+1) + \underline{a}(-1)^{I+\frac{1}{2}}(I+\tfrac{1}{2}) \delta_{K,\frac{1}{2}} \right. \tag{1}$$

$$\left. - [K(K+1) + \underline{a}(-1)^{K+\frac{1}{2}}(K+\tfrac{1}{2}) \delta_{K,\frac{1}{2}}] \right\}$$

where $\mathcal{I}$ is the moment of inertia of the nuclear deformation. The decoupling parameter $\underline{a}$ depends on the intrinsic structure of the nucleus and only enters into equation 1 when $K = \frac{1}{2}$. Since K is only approximately a good quantum number, the expression for the energy spacings actually will involve higher order terms of E_{rot} to account for interactions of the rotational motion with the intrinsic states. Transitions between levels must obey the selection rules

$$|I_i - I_f| \leq L \leq I_i + I_f \qquad \pi_i \pi_f = (-1)^L \quad \text{EL}$$

$$|K_i - K_f| \leq L \qquad \pi_i \pi_f = (-1)^{L+1} \quad \text{ML}$$

where I represents the nuclear spin, π the parity, K the K quantum number of the levels, and L the multipole order of the transition. EL and ML denote the electric and magnetic multipolarity, respectively.

Recently Nilsson (3) has calculated nuclear independent particle levels and wavefunctions assuming a spheroidal harmonic potential with spin-orbit coupling. These calculations enable the prediction of the spins and parities of some of the groundstates and low lying excited states in odd A deformed nuclei (4). Nilsson's results have proved useful for

identifying some of the intrinsic levels in the nuclear level schemes described in this thesis.

An experimental investigation of the spectra of two odd A nuclei, Tm^{169} and Lu^{175} has been undertaken in order to obtain precise values for the observed energy levels, the spins and parities of the levels, and the intensities of transitions between levels. In the study of the spectra of these two nuclei, rotational characteristics predicted by the unified model have been observed.

The radiations from Tm^{169} and Lu^{175} have been studied using the 2-meter curved-crystal gamma-ray diffraction spectrometer (5)(6), the homogeneous-field ring-focusing beta-ray spectrometer (7)(8), and a semicircular homogeneous-field beta-ray spectrometer (9).

Ytterbium as found in nature consists of seven stable isotopes, Yb^{168}, Yb^{170}, Yb^{171}, Yb^{172}, Yb^{173}, Yb^{174} and Yb^{176} (10). Of these isotopes, three, Yb^{168}, Yb^{174} and Yb^{176} form unstable isotopes following single neutron capture. By neutron capture ${}_{70}Yb^{168}_{98}$ forms Yb^{169}_{99} which decays by electron capture to ${}_{69}Tm^{169}_{100}$, the only stable isotope of thulium. ${}_{70}Yb^{174}_{104}$ forms ${}_{70}Yb^{175}_{105}$ which decays by beta-emission to the stable isotope ${}_{71}Lu^{175}_{104}$, and ${}_{70}Yb^{176}_{106}$ forms ${}_{60}Yb^{177}_{107}$ which decays by beta-emission to ${}_{71}Lu^{177}_{106}$, which in turn decays by beta-emission to the stable isotope ${}_{72}Hf^{177}_{105}$. The Yb^{177} decay was not studied because of its short half-life (1.8 hours). The 6.8 day activity of Lu^{177} produced by the decay of Yb^{177} was

weak. It had been studied previously in this laboratory using neutron irradiated lutecium (11). In the present experiments, only the two strongest lines at 112.97 and 208.36 kev could be observed.

Following the electron capture from Yb^{169}, the Tm^{169} nucleus emits gamma-rays and internal conversion electrons as it decays to its groundstate. Similarly, part of the beta-decay of Yb^{175} goes to excited states of Lu^{175}, and gamma-rays and internal conversion electrons are emitted during the de-excitation to the groundstate.

From measurements of the energies of the emitted gamma-rays and from determinations of the multipolarities of the observed transitions, precision energies of some of the low lying energy levels of Tm^{169} and Lu^{175} have been determined.

This thesis describes the results from observations of Tm^{169} and Lu^{175} nuclear spectra. The work begins with the presentation and description of the experimental gamma-ray and beta-ray spectrometer measurements in Parts II and III. The analysis and interpretation of the Tm^{169} and Lu^{175} measurements according to present theoretical ideas follow in Parts IV and V. In the appendices are found technical data about the radioactive sources, measurements obtained in the course of the experiments which are not directly related to the Tm^{169} and Lu^{175} energy levels, and tables and data used in the analysis of the Tm^{169} and Lu^{175} levels.

PART II

GAMMA-RAY ENERGY AND INTENSITY MEASUREMENTS

GAMMA-RAY ENERGY AND INTENSITY MEASUREMENTS

A TECHNIQUE

The energies and gamma-ray intensities of most of the observed transitions in Tm^{169} and Lu^{175} were measured using the curved-crystal spectrometer. Recently some changes were made in the detecting apparatus of the spectrometer in order to increase the detecting efficiency and to reduce background. A brief description of the present detector follows.

After passing through the collimator, the gamma-rays reach a NaI crystal, three inches in diameter and two inches thick, mounted on the face of a DuMont 6364 photomultiplier. The pulses from the photomultiplier are fed, after suitable amplification, to a single channel pulse-height analyzer which is adjusted to the photopeak of the observed gamma-line. The output pulses are either registered directly by a scalar and a printer, or are fed into a linear counting-rate meter and displayed on a chart recorder. The principal advantages of the present detecting system are to provide a better signal-to-noise ratio than that of the detector used earlier and to permit a much more reliable interpretation of intensity data.

Energy Measurements

Each determination of a gamma-line energy was made by matching the line profiles obtained by reflection from opposite

sides of the (310) planes of the curved quartz lamina. Usually the spectrometer is calibrated with the W Kα lines emitted by a Ta^{182} source. For the present measurements, however, an indirect calibration was more practical. Using a neutron irradiated Hf sample decaying into Lu^{175} and Ta^{181}, the wavelengths of the Lu Kα lines were first measured (see Appendix II) with the well known* Ta Kα lines as a standard. For all subsequent energy determinations, the Lu Kα lines could be used as a secondary standard. It is believed that such a procedure does not introduce any serious lack of precision in the measured energies, and it has the advantage of permitting all measurements without removing the radioactive source from the spectrometer.

The energy resolution, $\frac{\Delta E}{E}$, of the gamma-ray spectrometer is given for the present measurements by $\frac{\Delta E}{E} = 0.3 \times 10^{-4} E$, where E is the energy in kev and ΔE is the line profile width at half-maximum. Except for low intensity lines, the absolute uncertainties assigned to the energy values correspond to 1/20 of the width of the line profiles at half-maximum, or 10 e.v., whichever is larger.

---

*The wavelengths given by Ingelstam (12) for the Ta Kα lines are in excellent agreement with the values obtained in this laboratory by comparison of the W Kα lines and the Ta Kα lines emitted by a Ta^{182} source.

Intensity Measurements

The relative intensities of the gamma-rays were obtained with the curved-crystal spectrometer in the following way. The spectrometer was set at the Bragg angle corresponding to the peak of the line being studied and the pulse height spectrum of the NaI detector was recorded. The total number of counts recorded in the photopeak is proportional to the relative intensity of the gamma-line after the corrections for self absorption in the source, detector efficiency and curved-crystal reflectivity are applied. The total number of counts in the photopeak, or the area under the photopeak curve has to be used as a measure of the intensity rather than the maximum counting-rate of the photopeak because of the energy dependence of the resolution of a scintillation spectrometer. When the escape peak is resolved from the photopeak, its number of counts has to be added.

The corrections to be applied for the self absorption of the cylindrical source have been given by Murray (13). The NaI crystal photoelectric efficiency was calculated using the method of Maeder, Müller and Wintersteiger (14).

Curved-crystal Reflectivity

Lind (15) has measured the integrated reflection coefficient of a 1 mm thick curved quartz crystal over the wavelength range of 9 x.u. to 500 x.u. with the result that the energy dependence for the coefficient was about $1/E^2$, where E

denotes the gamma-ray energy. Also it has been found that the integrated reflection coefficient varies from a $1/E$ energy dependence for unstressed quartz lamina to the $1/E^2$ dependence for the stressed 1 mm thick lamina (16). The curved quartz crystal used for the measurements presented here, however, was 2 mm thick, and since the stresses in the 2 mm thick curved crystal are larger than those in the 1 mm thick curved crystal, it seemed possible that the reflectivity of the 2 mm crystal might have an energy dependence other than $1/E^2$. Therefore an attempt has been made to study the reflectivity energy dependence by measuring the reflectivity of the 2 mm crystal at a few gamma-ray energies.

For a few gamma-ray energies direct determinations of the reflection coefficient were made. These determinations are possible for gamma-rays whose photopeaks are resolved in the direct beam NaI pulse-height spectrum. For example using the Tm^{169} 307.7 kev gamma-ray, the procedure was the following. First the curved-crystal spectrometer was set at zero Bragg angle so that the NaI crystal was detecting the direct beam of gamma-rays, and the pulse-height spectrum was recorded. The pulse-height spectrum shows a well resolved photopeak due to the 307.7 kev line (fig. 4). Then the spectrometer was set at the Bragg angle corresponding to the peak of the reflected line profile of the 307.7 kev gamma-ray and the pulse height spectrum due to the reflected gamma-rays was recorded. The total number of counts, I_d, in the photopeak

of the 307.7 kev gamma-ray in the direct beam spectrum, and the total number of counts, I_r, in the reflected 307.7 kev photopeak were determined. The ratio I_r/I_d is a measure of the reflection coefficient at 307.7 kev. Corrections for self-absorption and detector efficiency had not to be applied since the same coefficients for these corrections would apply to both the direct beam and the reflected beam measurements and would cancel out in the ratio I_r/I_d. A similar procedure was carried out with the Tm^{169} 177.24 and 197.97 kev gamma-rays. In the case of these two gamma-rays, however, their individual photopeaks in the direct beam spectrum were not resolved. Therefore the total number of counts in their common photopeak, which was resolved from the other photopeaks, was distributed between them according to their relative intensities as determined from the external conversion measurements with the beta-ray spectrometer (see Part III).

The ratio I_r/I_d was determined at two more points using the Yb^{170} 84.26 kev gamma-ray from a radioactive Tm^{170} source and the 343.4 kev gamma-ray from a radioactive Hf^{175} source. The 84.26 kev gamma-ray is the only gamma-ray in the Yb^{170} spectrum, and its photopeak is resolved from the x-ray photopeak. It was possible to resolve completely the photopeak of the 343.4 kev gamma-ray in the direct beam pulse-height spectrum and to avoid overloading the detector by placing a 1/8" lead absorber immediately in front of the NaI crystal during the measurements of both I_r and I_d.

The Tm^{170} source had the same effective width as the Yb^{169} source so that the I_r/I_d values from these two sources corresponded. The Hf^{175} source, however, was 0.006" in diameter while the Yb^{169} source was 0.008" in diameter (see Appendix II) so that I_d for 343.4 kev was increased by the factor 4/3 according to a result given by Lind (15) in order that the I_r/I_d value at 343.4 kev would correspond to that from a 0.008" diameter source. The plot (fig. 1) of the various experimentally obtained I_r/I_d values shows an energy dependence close to $1/E^2$.

As a rough check an independent determination of the relative intensities of some of the gamma-rays emitted by Tm^{169} was made with the beta-ray spectrometer using the photoelectric effect in an external converter (see Part III). Let I_g be the relative intensity of a gamma-line obtained by the curved-crystal spectrometer, applying all corrections except that for crystal reflectivity. If I_e is the relative intensity of the same gamma-ray obtained from external conversion, then the ratio I_g/I_e is proportional to the reflectivity of the 2 mm crystal. This ratio is plotted in fig. 2 for the 109.78, 130.53, 177.24, 197.97 and 307.7 kev gamma-rays from Tm^{169}. Within the experimental uncertainties fig. 2 indicates that the curved-crystal reflectivity varies more like $1/E^2$ than like $1/E$ or $1/E^3$.

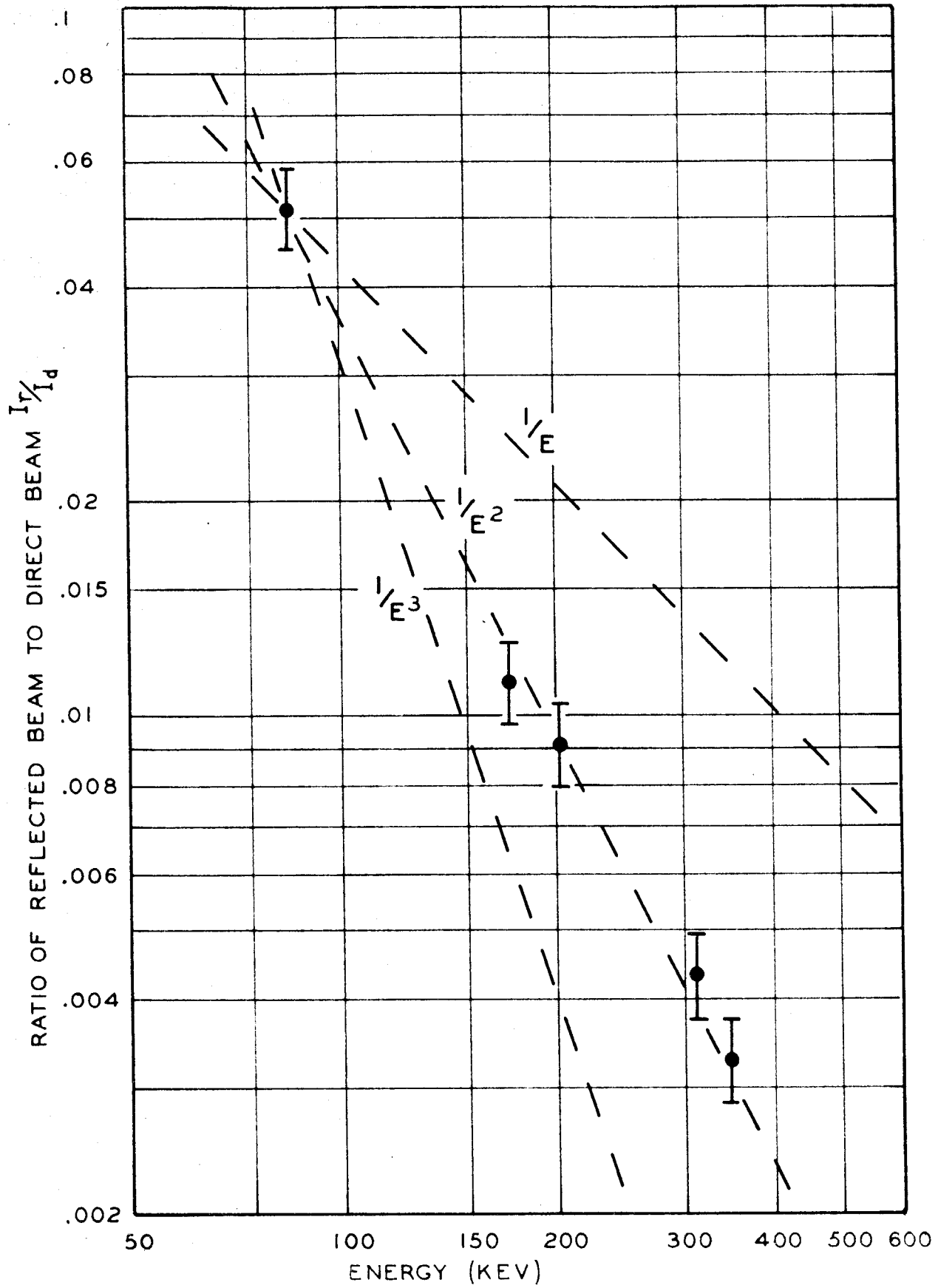

Figure 1. Curved-crystal reflectivity for 0.008" diameter radioactive source.

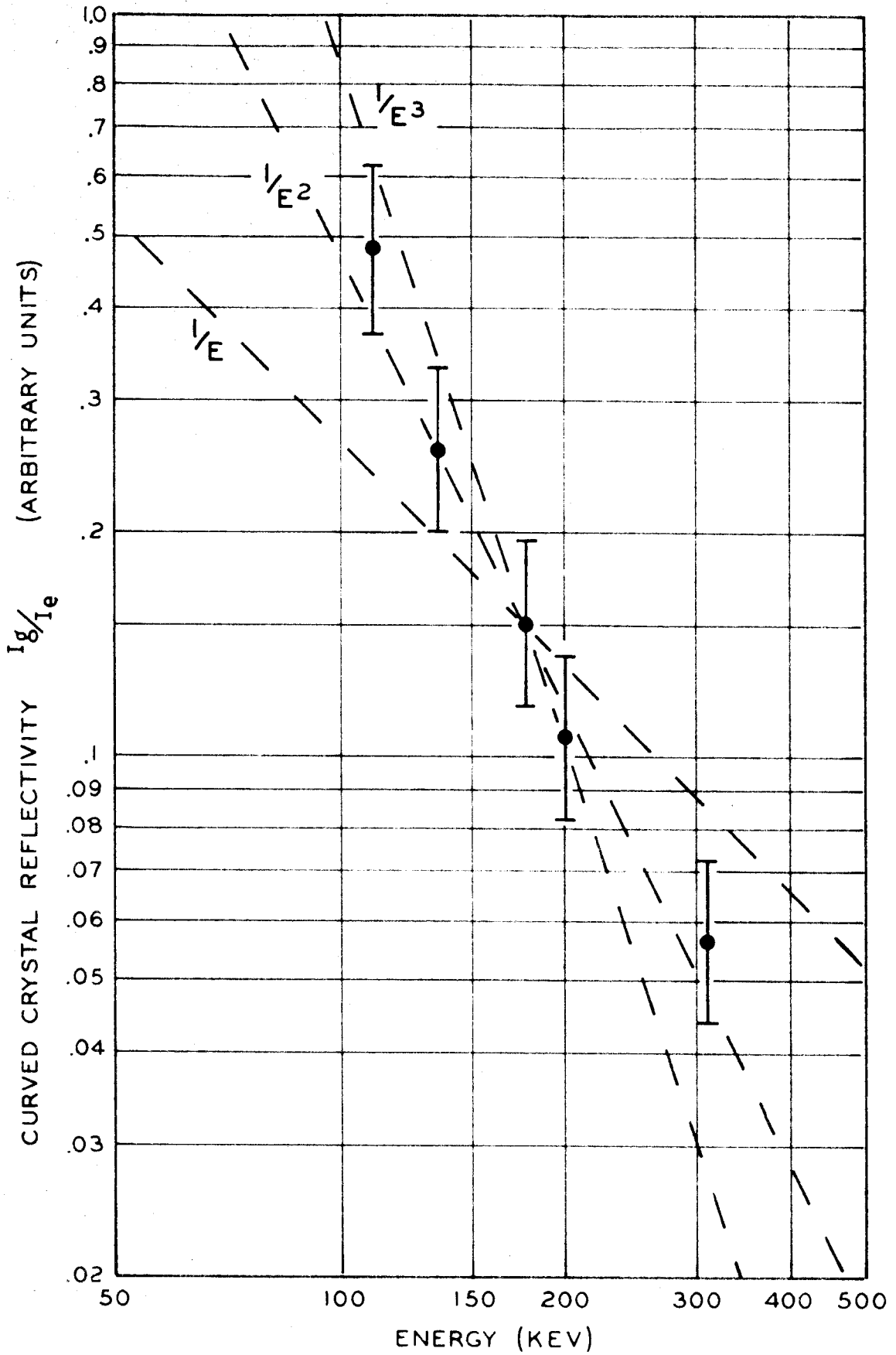

Figure 2. Energy dependence of curved-crystal reflectivity.

As a result of the preceding data, the coefficient used to correct the measured relative intensities for the reflectivity of the curved crystal in the gamma-ray spectrometer was $1/E^2$. As new sources are studied, additional points of I_r/I_d will be determined to extend the range and the precision of the experimentally determined reflection coefficient.

B RESULTS

The results obtained with the curved-crystal spectrometer are presented in Table 1 and Fig. 3.

Table 1. Energies and Relative Intensities of Gamma Rays from Tm^{169} and Lu^{175}

	Energy kev	Relative Intensities Tm^{169}	Lu^{175}
A.	63.12 ± 0.01	650.	
B.	93.60 ± 0.04	44.	
C.	109.78 ± 0.02	220.	
D.	113.81 ± 0.02		310.
E.	118.20 ± 0.03	26.	
F.	130.53 ± 0.03	150.	
G.	137.65 ± 0.05		22.
H.	144.85 ± 0.03		59.
I.	177.24 ± 0.05	310.	
J.	197.97 ± 0.06	510.	
K.	240.4 ± 0.7	11.	
L.	251.3 ± 0.5		38.
M.	261.0 ± 0.5	82.	
N.	282.57 ± 0.13		620.
O.	307.7 ± 0.5	180.	
P.	396.1 ± 0.3		1000.

Table 1 contains measured energies and relative intensities of the observed gamma-ray transitions in Tm^{169} and Lu^{175}. The gamma-ray energies were measured with the curved-crystal spectrometer.

All energies in Table 1 except K_1 were measured with a resolution $\frac{\Delta E}{E} = 0.3 \times 10^{-4}$ E where E is the energy in kev. K_1 was measured with a 50 mg Yb source, the spectrum from which is shown in fig. 3. The resolution obtained from this source was $\frac{\Delta E}{E} = 0.6 \times 10^{-4}$ E because of its larger geometrical size in the direction of dispersion of the spectrometer. Except for low intensity lines, the assigned energy uncertainties are 1/20 of the line profile width at half-maximum or 10 e.v., whichever is larger.

To account for the decay, the Tm^{169} and Lu^{175} relative intensities were normalized to measurements on a specific date. The estimated uncertainties in the relative intensities are $\pm$ 15% of the value for intensities greater than 200, $\pm$ 30% otherwise.

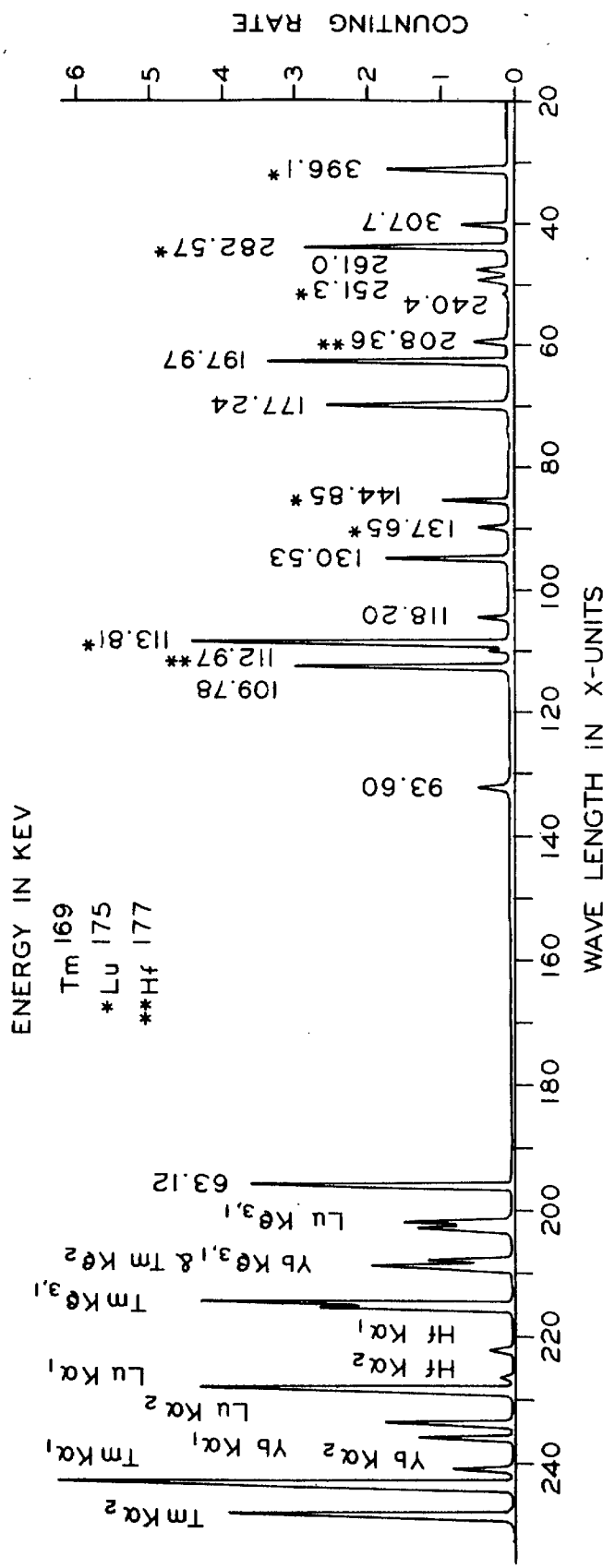

Figure 3. Gamma-ray and x-ray spectrum from 48 to 400 kev emitted from the 50 mg Yb source.

Figure 3 shows the complete gamma-ray spectrum as observed with the curved-crystal spectrometer. The source consisted of 50 mg of Yb_2O_3 (see Appendix I), irradiated for 19 days at a flux of 5 x 10^{13} neutrons/cm^2/sec in the Phillips Petroleum Company Materials Testing Reactor at Arco, Idaho. When placed in the spectrometer, the Yb source had an activity of approximately one curie.

In this figure the ordinate is proportional to the observed counting rate, which was recorded by a chart recorder from the output of a linear counting-rate meter. The wavelength setting of the spectrometer was changed 0.04 x.u. every 12 seconds. Approximately 20 hours were required to explore the region from 20 x.u. to 255 x.u. Of course, the peaks of the lines do not represent the actual relative intensities of the gamma-ray transitions since no corrections have been made for self-absorption in the source, curved crystal reflectivity, detector efficiency, or half-lives.

Each gamma-line is labeled with its energy in kev obtained from matching line profiles. In addition to gamma-rays from transitions in Tm^{169} and Lu^{175} and the accompanying x-rays, the 112.97 and 208.36 kev gamma-lines from Hf^{177} are observed along with the Hf $K\alpha_1$ and $K\alpha_2$ x-rays. The two gamma-lines represent the two strongest transitions in Hf^{177} (11). Since the Yb source was 99.8% pure, containing no detectable amount of Lu, the Hf^{177} undoubtedly arises from the 1.8 hour beta-decay of Yb^{177} into Lu^{177} followed by the 6.8 day beta-decay

of Lu^{177}.

The Kα and Kβ groups of x-rays from $_{69}Tm$, $_{70}Yb$, and $_{71}Lu$ can be noted. The group labeled Yb K$\beta_{3,1}$ also contains the Tm Kβ_2 line. Similarly the Lu K$\beta_{3,1}$ group contains the Yb Kβ_2 line. The Lu Kβ_2 line is not resolved from the Tm^{169} 63.12 kev line in this figure. The Tm K x-rays arise following both the K-capture of Yb^{169} and internal conversion in the Tm^{169} K-shell. Due to the K-capture and due to the fact that several transitions in the Tm^{169} de-excitation are strongly K converted, the Tm K x-rays are more intense than any of the gamma-lines in the Tm^{169} spectrum. The Lu K x-rays arise almost entirely following K-conversion in Lu^{175} nuclear transitions, while the Yb K x-rays are due to electronic de-excitation following ionization in the K-shell by gamma-rays or energetic electrons.

The width at half-maximum of the gamma-line profiles obtained with the 50 mg Yb source was 0.75 x.u. The precision values of the gamma-ray energies were obtained using a source which provided line profiles having 0.35 x.u. width at half-maximum, thus giving roughly two times better resolution.

Figure 4 shows a NaI pulse-height spectrum of gamma-ray transitions from Tm^{169} compared with the curved-crystal spectrum of fig. 3, replotted on the energy scale. Since the widths at half-maximum of the line profiles are approximately constant on the wavelength scale when the spectrum is plotted against the energy E, the widths of the profiles

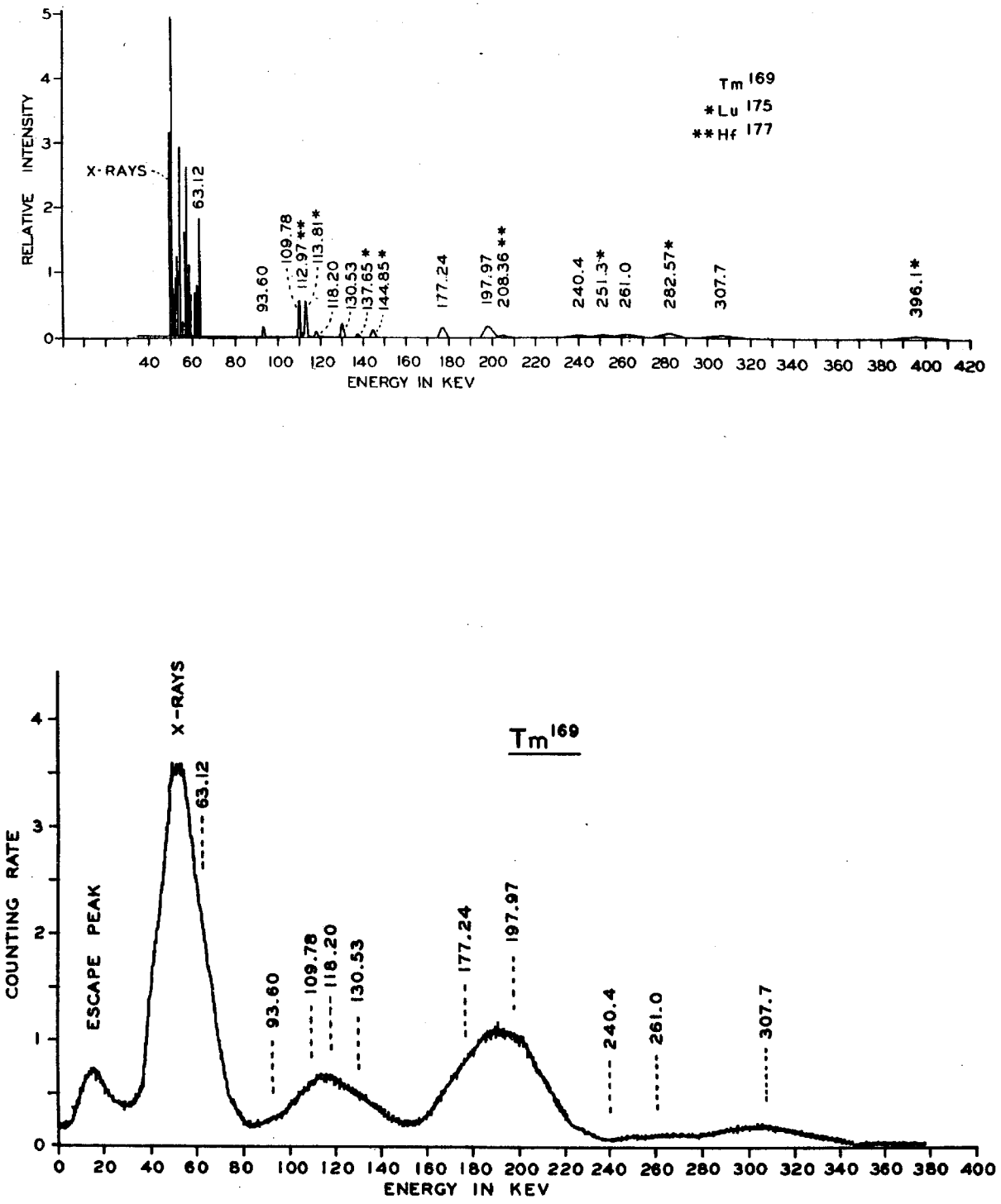

Figure 4. Comparison of resolutions obtained by curved-crystal spectrometer and NaI scintillation spectrometer.

increase as E^2. The Tm^{169} pulse-height spectrum was obtained from the direct beam of the curved-crystal spectrometer by setting the spectrometer at zero Bragg angle and recording the counting rate on a chart recorder as the base-line voltage of the pulse-height analyzer was increased at a uniform rate. It should be noted that the pulse-height spectrum contains gamma-rays only from Tm^{169}, while the curved-crystal spectrum shows lines from Tm^{169}, Lu^{175}, and Hf^{177}.

PART III

BETA-RAY SPECTROMETER MEASUREMENTS

BETA-RAY SPECTROMETER MEASUREMENTS

A TECHNIQUE

The energies and relative intensities of internal conversion electrons from transitions in Lu^{175} and Tm^{169} were measured with beta-ray spectrometers. By utilizing the photoelectric effect in external converters, it was also possible to measure the relative intensities of some of the gamma-rays emitted by the Tm^{169} nucleus.

Two beta-ray spectrometers were employed for observing the internal conversion electrons. One, the ring-focusing spectrometer, is equipped with a Geiger-counter having a 0.7 mg/cm^2 mica window, which transmits electrons down to about 25 kev. This instrument was used for observing the Yb^{175} beta spectrum and Tm^{169} and Lu^{175} conversion lines above 35 kev. The other, a semicircular homogeneous-field spectrometer, enabled the measurement of the Tm^{169} 8.42 and 20.75 kev transitions, which were below the range of the other instruments (the curved-crystal spectrometer range extends from about 30 kev to 1.5 Mev, while the ring-focusing spectrometer range is from 25 kev to 5 Mev). The homogeneous magnetic field of the semicircular spectrometer is produced by a set of Helmholtz coils 67 cm in diameter. The radius of the electron trajectories is 12 cm. The detector is a Geiger counter with a thin formvar window, usually 10 to

20 micrograms/cm^2. With a 10 microgram/cm^2 window, the Tm^{169} 63.12 kev K-line was clearly detected at 3.76 kev (fig. 5). Observations of Tm^{169} conversion lines from 3.7 to 110 kev were made with the semicircular spectrometer.

Momentum resolutions, $\frac{\Delta p}{p}$, where p is the electron momentum and Δp is the momentum width of the line profiles at half-maximum of 0.65%, 0.35% and 0.15% were obtained with the ring-focusing spectrometer. Low energy measurements with the semicircular spectrometer were carried out with a resolution of 0.75%. For this resolution, the source and counter window had the dimensions 0.12 cm x 4 cm.

Internal Conversion Line Relative Intensities

The multipolarities of the nuclear transitions were determined by their K shell and L sub-shell conversion coefficients. In evaluating relative intensities from the observed conversion peaks, it was necessary to apply corrections for absorption by the 0.7 mg/cm^2 mica window of the counter. For this purpose the empirical curve obtained by Murray (13), of transmission versus energy was used. In most cases the height of the peak of the conversion line rather than the area was taken to be proportional to the line intensity.

Gamma-ray Intensities by External Conversion

The relative intensities of the Tm^{169} 109.78, 130.53, 177.24, 197.97 and the 307.7 kev gamma-rays were obtained with lead and uranium photoconverters. The uranium L_I, L_{II}

and L_{III} shell photopeaks due to the 109.78, 130.53, and 177.24 kev gamma-rays were observed and their intensities compared, while the lead K-shell photopeaks due to the 177.24, 197.97 and 307.7 kev gamma-rays were measured and their intensities compared. The uranium converter was a small disc of uranium metal 0.35 mg/cm^2 thick and 3.0 mm in diameter, obtained by evaporation on an aluminum foil. The lead converter, also prepared by evaporation on an aluminum backing, was 0.8 mg/cm^2 thick and 3.0 mm in diameter. Momentum resolution of 0.65% was obtained for the external conversion measurements.

In addition to the corrections for absorption in the counter window, corrections were applied for the gamma-ray self absorption in the source and for the variation of the photoelectric absorption coefficient of the converter. The self absorption correction was carried out in the same way as for the curved-crystal spectrometer; namely, by considering the photoelectric absorption by the source material at the particular gamma-ray energy in question. The external converter photoelectric absorption coefficients in the case of the lead K-shell were taken from curves by Stobbe (17), while for the uranium L sub-shells the coefficients were computed from formulas derived by Hall and by Stobbe (18) (see fig. 10, Appendix I). Table 2 gives a comparison of the gamma-ray intensities obtained from external conversion and those obtained from the gamma-ray spectrometer. The two sets of relative intensity values are normalized at 177.24 kev. The discrepancies are well within the expected uncertainties of the external conversion measurements.

Table 2. Comparison of Relative Intensities Obtained with Curved-crystal Spectrometer and by External Conversion with Ring-focusing Beta-ray Spectrometer

Gamma-ray energy kev	Curved crystal relative intensities	External conversion relative intensities
109.78	220	180
130.53	150	160
177.24	310	310
197.97	510	570
307.7	180	160

B RESULTS

Results obtained with the ring-focusing spectrometer and the semicircular spectrometer are presented in Table 3 and figures 5 and 6.

Table 3. Internal Conversion Lines in Tm^{160} and Lu^{175}

Bρ Gauss-cm	Electron energy kev	Relative intensities	Identification Tm^{169}	Identification Lu^{175}
* 207.3	3.76	(a)	63.12 K	
* 265.1	6.14	-	8.42 M_I	
* 274.4	6.58	-	8.42 $M_{II} + M_{III}$	
* 302.9	8.01	-	8.42 N_I	
* 310.4	8.40	-	8.42 N_{IV} -, O	
* 349.5	10.63	-	20.75 L_I	
* 357.6	11.13	-	20.75 L_{II}	
* 373.2	12.11	-	20.75 L_{III}	
* 461.7	18.42	-	20.75 M	
* 482.1	20.05	-	20.75 N	
* 634.4	34.25	210.	93.60 K	
* 775.2	50.37	930.	109.78 K	
776.3	50.50	1000.		113.81 K
* 796.4	53.03	120.	63.12 L_I	
* 799.5	53.42	30.	63.12 L_{II}	
* 807.6	54.46	40.	63.12 L_{III}	
* 841.1	58.83	34.	118.20 K	
* 859.8	61.33	38.	63.12 M	
* 871.0	62.85	11.	63.12 N	
* 930.1	71.13	160.	130.53 K	
953.4	74.51	44.		137.65 K
1000.0	81.45	12.		144.85 K
*1014.0	83.59	36.	93.60 L_I	
*1061.8	91.04	12.	93.60 M	
*1114.8	99.59	150.	109.78 L_I	
1136.5	103.18	240.		113.81 L_I
1138.5	103.51	61.		113.81 L_{II}
1144.5	104.51	80.		113.81 L_{III}
*1161.1	107.30	(b)	109.78 M	
*1165.4	108.02	-	118.20 L	
*1174.3	109.53	-	109.78 N	
1186.2	111.57	80.		113.81 M
1195.2	113.11	27.		113.81 N
1222.9	117.93	310.	177.24 K	
1238.4	120.64	92.	130.53 $L_I + L_{II}$	

Table 3. Continued

Bρ Gauss-cm	Electron energy kev	Relative intensities	Identification Tm^{169}	Identification Lu^{175}
1244.0	121.63	79.	130.53 L_{III}	
1271.7	126.56	(b)		137.65 L_I
1281.4	128.30	36.	130.53 M	
1291.3	130.08	12.	130.53 N	
1337.4	138.53	390.	197.97 K	
1488.2	167.37	56.	177.24 L_I	
1526.6	174.99	16.	177.24 M^I	
1589.3	187.67	70.	197.97 L_I	
1631.1	196.26	18.	197.97 M^I	
1659.	202.	-	261.0 K	
1743.	219.9	36.		282.57 K
1873.	248.3	14.	307.7 K	
1978.	271.8	6.		282.57 L
2094.	298.5	4.	307.7 L	
2128.	306.3	1.	307.7 M	
2240.	332.8	130.		396.1 K
2456.	385.3	24.		396.1 L
2490.	393.6	6.		396.1 M

[a]No relative intensity values were given for lines 63.12 K through 20.75 N because of the uncertainty in the energy dependence of the semicircular spectrometer counter window absorption. However, the relative intensity ratios of the 20.75 L_I, L_{II}, and L_{III} lines are:

$$\alpha L_I : \alpha L_{II} : \alpha L_{III} = 20 : 2.5 : 1$$

The ratio of 20.75 M and N lines is:

$$\alpha_M : \alpha_N = 3.4 : 1$$

[b]No relative intensity values are given for the 109.78 M, 118.20 L, 109.78 N, or 137.65 L lines since they were not sufficiently resolved.

Table 3 lists $B\rho$ in gauss-cm, the energy in kev and the measured relative intensities of the observed internal conversion electrons from nuclear transitions in Tm^{169} and Lu^{175}.

The conversion lines marked with * were observed with the semicircular beta-ray spectrometer. All conversion lines above the 20.75 N line were observed with the ring-focusing spectrometer. The assigned uncertainties to the measured relative intensities are $\pm$ 25% for lines with intensities greater than 20, $\pm$ 50% otherwise.

The Tm^{169} and Lu^{175} conversion line relative intensities are normalized to correspond to measurements taken with the Yb source at the same time as the corresponding gamma-ray relative intensity measurements (Table 1). In order to correlate intensities, the Lu^{175} 137.65 and 144.85 kev and the Tm^{169} 130.53 kev gamma-rays were measured with the curved-crystal spectrometer, while simultaneously the relative intensities of the corresponding K-conversion lines were measured with the ring-focusing beta-ray spectrometer.

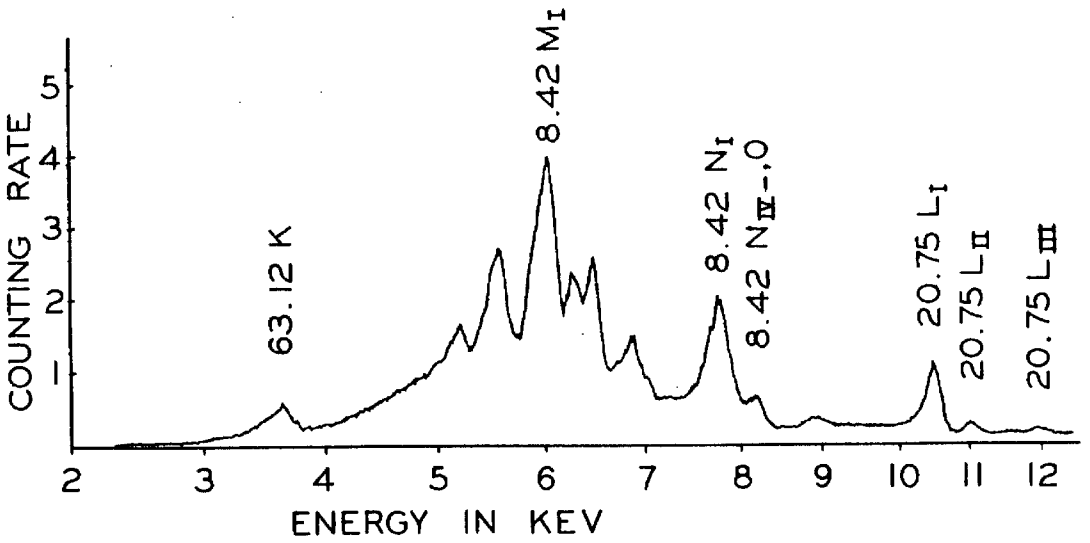

Figure 5. Conversion line and L-Auger spectrum from Tm^{169} from 3 to 12.5 kev observed with the semicircular spectrometer.

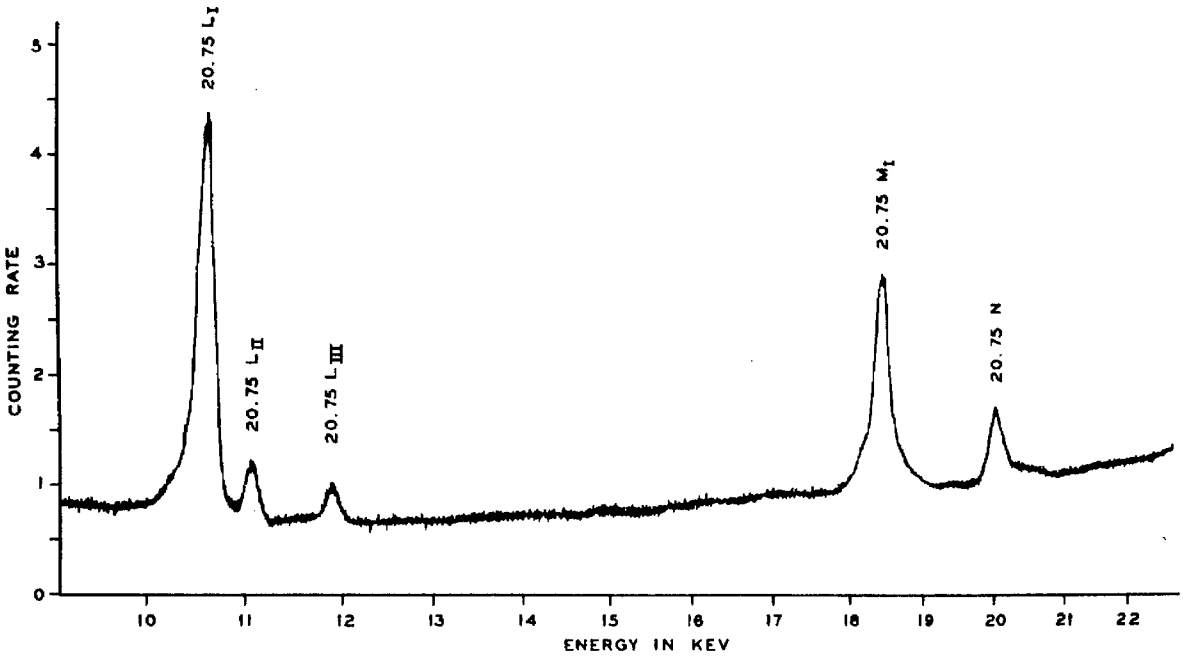

Figure 6. Conversion lines of the Tm^{169} 20.75 kev transition observed with the semicircular spectrometer.

Figure 5 shows the Tm^{169} spectrum from 3 to 12.5 kev as observed with the semicircular homogeneous-field beta-ray spectrometer. The unlabeled peaks are principally L-Auger lines. To identify the Tm L-Auger lines in this spectrum, an independent study of the Lu L-Auger spectrum emitted by a Hf^{175} source has been undertaken. In the spectrum of Lu^{175} no conversion electrons at low energies are present.

The conversion lines from the Tm^{169} 20.75 kev transition observed with the semicircular spectrometer are shown in Fig. 6.

C COINCIDENCE MEASUREMENTS

Coincidences between conversion electrons and gamma-rays were recorded using the ring-focusing spectrometer with a NaI scintillation crystal placed directly behind the source disc. The ring-focusing spectrometer was set at the peak of the Tm^{169} 130.53 K-line and the coincidences were recorded as a function of the scintillation spectrum settings. The coincidences recorded showed that the Tm^{169} 177.24 kev transition is in coincidence with the 130.53 kev transition, while the 197.97 and 307.7 kev transitions are not, supporting the proposed level scheme for Tm^{169} (see Part IV).

D Yb^{175} CONTINUOUS BETA SPECTRUM

The end-point of the high energy component of the Yb^{175} beta-decay was determined to be 465 ± 5 kev from a Kurie plot of the spectrum. This value agrees closely with the value 468 ± 5 kev obtained by Mize, et al. (19). Taking into account the 102 hour half-life of the decay, a log ft = 6.4 resulted (20).

E SEARCH FOR POSITRONS IN Yb^{169} DECAY

An attempt to observe a positron spectrum in the decay of Yb^{169} was carried out with the ring-focusing spectrometer. No positrons were observed and an upper limit of 10^{-4} positron

per decay could be set on the intensity of Yb^{169} positron emission. From this result an upper limit of $\sim$ 1.3 Mev can be set for the electron capture disintegration energy.

PART IV

LEVELS IN Tm^{169}

LEVELS IN Tm^{169}

A SUMMARY OF RESULTS AND LEVEL SCHEME

The first observation of the electron-capture decay of Yb^{169} was reported by Bothe in 1946 (21). Subsequent investigations of the level scheme of Tm^{169} have been carried out by Martin, et al. (22) and by Cork and coworkers (23)(24). DeBenedetti and McGowan (25) have reported an isomeric transition in the de-excitation of the Tm^{169} nucleus. Measurements by several investigators have indicated the lifetime of the metastable state to be close to 0.7 microsecond (26)(27).

Recently Johansson (28) has studied the Tm^{169} level scheme by performing gamma-gamma coincidences with scintillation spectrometers. Johansson found the 63.12 and 93.60 kev gamma-rays in prompt coincidence with the Tm x-rays and all other gamma-rays in delayed coincidence with the x-rays. He concluded that the 93.60 kev transition immediately precedes the 63.12 kev transition, which leads to the 0.7 microsecond metastable state.

Huus, et al. (29) have observed 110 and 120 kev transitions following Coulomb excitation of Tm^{169}. From a study of the shape of the excitation of the 110 kev radiation, they have pointed out the possibility of a first excited state at around 10 kev.

A complete level scheme giving spins and parities of all observed levels has not been proposed by the previous investigators (22)(24)(28). From the present investigation it is possible to establish a more complete level scheme of Tm^{169} and to assign the spins and parities to all observed levels.

The results of the present measurements are summarized in Table 4, and the proposed level scheme is given in Figure 7.

Table 4. Comparison of Experimental and Theoretical Conversion Coefficients

Tm^{169}

Initial and final levels	Energy kev	α_K Exp.	α_K Theo. E1	α_K Theo. E2	α_K Theo. M1	α_K Theo. M2	α_{L_I} Exp.	α_{L_I} Theo.	$\alpha_{L_I+L_{II}}$ Exp.	$\alpha_{L_I+L_{II}}$ Theo.	$\alpha_{L_{III}}$ Exp.	$\alpha_{L_{III}}$ Theo.	α_L Exp.	α_L Theo.	Total	I_γ	Decay fraction %	Multipole assignment
BA	8.42	-					-								-	-	(95)	(M1)
DC	20.75	-					-								-	-	(13)	(M1)
FE	63.12	-					-		0.12	0.12	0.03	0.04			1.04	650	90	E1
GF	93.60	2.4	[a]0.32 [b]0.33	1.4 1.16	3.65 3.2	27.5 27.0	0.42	[c]0.52							2.75	44	11	M1(+E2)
CB	109.78	2.1	0.21 0.22	0.88 0.83	2.35 2.0	16.0 15.0	0.34	0.33							2.57	220	54	M1
CA	118.20	0.66	0.175 0.18	0.73 0.70	1.90 1.60	12.5 11.5	-								1.60	26	5	E2
DB	130.53	0.55	0.135 0.14	0.550 0.543	1.42 1.23	8.8 8.2			0.31	0.29	0.27	0.21			1.25	150	23	E2
ED	177.24	0.51	0.063 0.062	0.23 0.23	0.62 0.52	3.05 2.8	0.09	0.08							0.62	310	35	M1
EC	197.97	0.40	0.047 0.047	0.17 0.17	0.46 0.38	2.1 1.95	0.07	0.06							0.48	510	51	M1
FD	240.4	-					-								0.03	11	1	(E1)
FC	261.0	-					-								0.03	82	6	(E1)
EB	307.7	0.04	0.015 0.015	0.05 0.05	0.135 0.115	0.49 0.45							0.01	0.02	0.05	180	13	E2

[a]The upper value of theoretical α_K was obtained from tables by Rose, et al. (30).

[b]The lower value of theoretical α_K was obtained from tables by Sliv (31).

[c]Theoretical M1 coefficient.

Table 4 gives conversion coefficient data, decay fractions and multipole assignments for the Tm^{169} transitions observed in the present experiments. The energies of all observed transitions except BA and DC were measured with the curved-crystal spectrometer. Transitions BA and DC were observed with the semicircular spectrometer and their measured conversion line energies (Table 3, Part III) agree well with those obtained by taking the corresponding differences of measured gamma-line energies. The value 8.42 $\pm$ 0.05 kev was obtained by subtracting CB from CA, while 20.75 $\pm$ 0.05 kev was obtained by subtracting CB from DB (see Tm^{169} level scheme, fig. 7).

The experimental conversion coefficient for a conversion line resulted from dividing the relative intensity of the conversion line (Table 2) by the relative intensity of the corresponding gamma-ray (Table 1). The ratios so obtained were then normalized to the theoretical value (30)(31) for the 130.53 kev K-conversion line. The 130.53 kev transition was chosen for normalization because it was a pure E2 transition.

Two sets of theoretical K-shell conversion coefficients are shown in Table 4. The upper value for each entry was obtained from tables computed by Rose, et al. (30), while the lower values were taken from tables computed by Sliv (31). The values by Sliv take into account the finite extension of the nucleus. It can be noted that the experimental coeffi-

cients for the 109.78, 177.24, and 197.97 kev transitions agree closely with the theoretical M1 values of Sliv, which are of the order of 15% lower than the values of Rose. Similar results in other nuclei have been previously reported by Wapstra and Nijgh (32).

With the exception of the L_{III}-shell coefficient, $\alpha_{L_{III}}$, the theoretical L-shell conversion coefficients were taken from tables by Rose (30) (Rose's tables for $\alpha_{L_{III}}$ were not available at the time of these experiments). $\alpha_{L_{III}}$ theoretical coefficients were obtained by interpolation of the data by Gellman, et al. (33).

α_{Total} denotes the total experimental conversion coefficient. Where the line intensities were too low, no experimental conversion coefficients are given. In these cases theoretical values for α_{Total} were inserted in Table 4.

The decay fractions were determined from $(1+\alpha_{Total})I_\gamma$ and normalized per disintegration. Decay fractions listed in parentheses were inferred from the level scheme (fig. 7).

The multipole assignments were obtained by comparing the experimentally determined K-shell and L sub-shell conversion coefficients with the theoretical values. Multipole assignments listed in parentheses were inferred from the level scheme (fig. 7). However, only E1 multipole assignments for the 240.4 and 261.0 kev transitions are consistent with the extremely weak K-conversion peaks. From the observed gamma-ray intensities (Table 1) of these transitions, readily observable K-conversion peaks would be expected for M1 or E2 multipolarity.

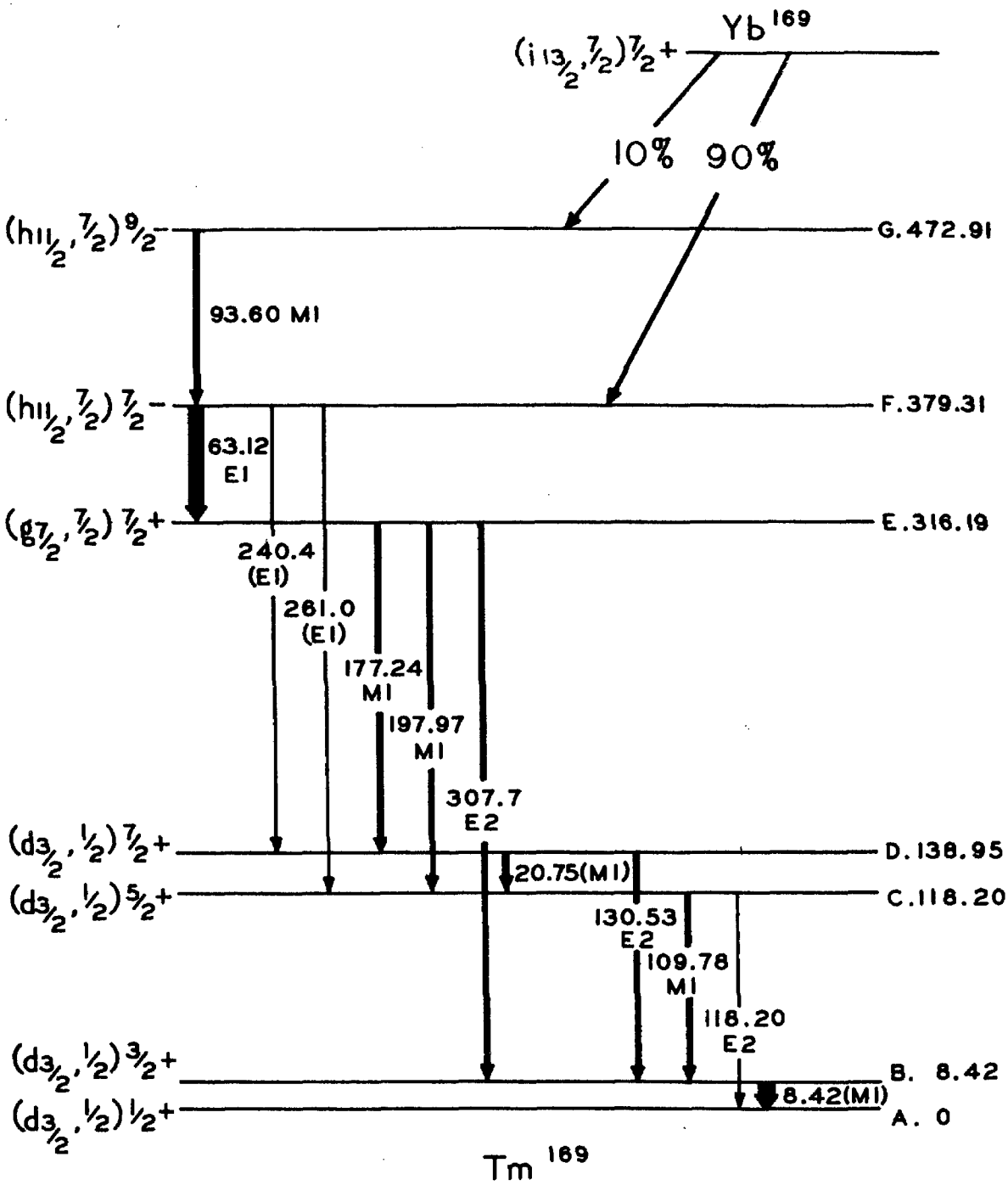

Figure 7. Tm^{169} level scheme.

In Fig. 7 the levels are labeled on the right with their energies in kev, which have been determined by combining those transition energies (Table 1) which have the smallest uncertainties.

Each level is labeled on the left with its spherical limit according to Nilsson's (3) calculations (Table 7, Appendix III), the K-quantum number, the spin and parity of the level.

The spins and parities of the levels have been assigned using the well known selection rules

$$|I_i - I_f| \leq L \leq I_i + I_f \qquad \pi_i \pi_f = (-1)^L \text{ EL}$$
$$\pi_i \pi_f = (-1)^{L+1} \text{ ML}$$

where L is the multipole order of the transition and π denotes parity of the levels. EL and ML denote the multipolarity.

The level scheme can be oriented from the observation of the 110 and 120 kev gamma-rays following Coulomb excitation (29)(34).

The 93.60 kev transition was placed above the 63.12 kev transition to agree with the coincidence measurement of Johansson (28).

From the decay fractions (Table 4) for the 63.12 and 93.60 kev transitions, the electron capture to level F was determined to be 90%, with 10% to level G. The observed electron capture to other levels is less than 10% of total decay.

The disintegration energy of the Yb^{169} electron capture has not been determined, but a rough estimate can be obtained from semi-empirical curves given by Way and Wood (35). According to these curves, the disintegration energy to the Tm^{169} groundstate is $\sim$ 1.1 Mev. From the proposed level scheme (fig. 7), the disintegration energies to levels G. and F. would then be $\sim$ 630 kev and $\sim$ 720 kev respectively. Taking into account the half-life of 31.8 days, and assuming the above disintegration energies and the experimentally determined branching ratios, log ft values of $\sim$8 and $\sim$7 result for the decay to levels G. and F. respectively. Because of the uncertainty in the disintegration energy these log ft values are approximate; however, they are in agreement with the decay being first forbidden.

B DISCUSSION

Interpretation of Levels

Calculations by Nilsson of individual particle energy levels in deformed nuclei enable the prediction of the spin and parities of the groundstates of many odd A isotopes (3)(4). The order of individual particle levels between the closed shells Z = 50 and Z = 82 as given by Nilsson for certain odd proton and odd neutron nuclei is shown in Tables 7 and 8 respectively (Appendix III).

The level ordering depends on the nuclear deformation, which can be deduced from Coulomb excitation measurements. For

Tm^{169} and Lu^{175} Mottelson and Nilsson (4) give a deformation parameter $\delta = 0.28$, and Tables 7 and 8 give the level order corresponding to this deformation.

The groundstate spin and parity for an odd proton nucleus is obtained by filling the extra-closed shell protons pairwise into the levels. The particle level occupied by the last odd proton will then describe the groundstate. Where adjacent particle levels in Table 7 or 8 are closely spaced, the order of filling of the levels may be ambiguous. In the case of Tm^{169} with 19 protons outside the closed shell at Z = 50, the groundstate is predicted to be either $(d_{3/2}, 1/2)$ or $(g_{7/2}, 7/2)$. Since the measured groundstate spin is 1/2 (36)(37), the groundstate is assumed to be described by $(d_{3/2}, 1/2)$.

Mottelson and Nilsson have interpreted levels A., B., C. and D. (fig. 7) as belonging to a rotational band based on the $(d_{3/2}, K = 1/2)$ groundstate (4)(38). From the spin and parity assigned to level E. (fig. 7) by the present measurements, this state can be interpreted as being the $(g_{7/2}, K = 7/2)$ particle excitation. Similarly, levels F. and G. can be interpreted as belonging to the rotational band based on the $(h_{11/2}, K = 7/2)$ particle excitation.

Energy Spacing of the Rotational Levels

Since Tm^{169} lies in a region of strong nuclear deformation, according to the Bohr-Mottelson unified model it should exhibit low lying rotational spectra (2). With the ground-

state having K = 1/2, the energy spacings of the rotational levels should be given by the anomalous spectrum:

$$E_{\frac{1}{2}}(I) = E_{\frac{1}{2}}^{(0)} + E_{\frac{1}{2}}^{(1)}\left\{I(I+1) + \underline{a}(-1)^{I+\frac{1}{2}}(I+\tfrac{1}{2})\right\} + E_{\frac{1}{2}}^{(2)}\left\{I(I+1) + \underline{a}(-1)^{I+\frac{1}{2}}(I+\tfrac{1}{2})\right\}^2 \quad (2)$$

where $E_{\frac{1}{2}}(I)$ denotes the energy above the groundstate of the member of the K = 1/2 band having spin I. $E_{\frac{1}{2}}^{(0)}$ is chosen so that the groundstate energy is zero. $E_{\frac{1}{2}}^{(1)}$ is equal to $\hbar^2/2\mathcal{I}$, where $\mathcal{I}$ is the moment of inertia of the nuclear deformation, and $E_{\frac{1}{2}}^{(2)}$ is the coefficient of a small second-order correction term. The decoupling parameter is denoted by $\underline{a}$.

If one neglects the second order correction term in equation 2 and determines $\underline{a}$, $E_{\frac{1}{2}}^{(0)}$ and $E_{\frac{1}{2}}^{(1)}$ by fitting the formula to the measured energies of states A., B. and C., one finds $\underline{a}$ = -0.7733, $E_{\frac{1}{2}}^{(0)}$ = -18.86 kev, and $E_{\frac{1}{2}}^{(1)}$ = 12.381 kev. With these values state D. with I = 7/2 is predicted to have an energy of $E_{\frac{1}{2}}(7/2)$ = 137.84 kev, which is of the order of 1 kev below the measured value of 138.95 kev. Thus it can be seen that a positive second-order correction term is required to fit the measured energies. Usually a negative second-order correction term is expected (2), however a positive correction term can be possible where there exist admixtures of states with different K num-

bers (39).

Again fitting equation 2 to the measured energies of states A, B, C, and D, while including the second-order term, the following values were obtained:

$$\underline{a} = -0.7680$$

$$E_{\frac{1}{2}}^{(0)} = -18.247 \text{ kev}$$

$$E_{\frac{1}{2}}^{(1)} = 11.969 \text{ kev}$$

$$E_{\frac{1}{2}}^{(2)} = + 0.03389 \text{ kev.}$$

These values resulted from solving the four simultaneous equations obtained by equating the values 0, 8.42, 118.20 and 138.95 kev to the expressions for E(1/2), E(3/2), E(5/2), and E(7/2) respectively. In solving the equations, several values of $\underline{a}$ were assumed and the first three equations solved for $E_{\frac{1}{2}}^{(0)}$, $E_{\frac{1}{2}}^{(1)}$ and $E_{\frac{1}{2}}^{(2)}$. Then the value of $\underline{a}$ which gave E(7/2) = 138.95 kev was determined graphically. Using the above parameters E(9/2) = 351.65 kev and E(11/2) = 387.37 kev can be predicted for the energies of the levels in the K = 1/2 band having I = 9/2 and I = 11/2. Transitions to or from these levels have not been observed.

If we assume levels G. and F. to be members of a K = 7/2 rotational band and use the same moment of inertia term ($E_{\frac{1}{2}}^{(1)}$ = 11.969 kev) obtained by fitting equation 2 to the

K = 1/2 band, an energy spacing between F. and G. of 107.72 kev is predicted by equation 1 (Part I). The difference between the predicted value (107.72 kev) and the measured value (93.60 kev) possibly can be accounted for by assuming that the K = 7/2 band is associated with a larger moment of inertia than the K = 1/2 band.

Transition Intensities

In order to compare the gamma-ray transition probabilities between nuclear energy levels, it is useful to remove the energy dependence and part of the multipole order dependence of the gamma-ray transition probability by defining a reduced transition probability.

Such a reduced gamma-ray transition probability, $B(L, I_i \rightarrow I_f)$, is defined by the equation

$$T_{i\rightarrow f}(L) = \frac{8\pi(L+1)}{L[(2L+1)!!]^2} \frac{1}{h}\left(\frac{\omega}{c}\right)^{2L+1} B(L, I_i \rightarrow I_f) \qquad (3)$$

where $T_{i\rightarrow f}(L)$ is the probability for a gamma-ray transition of multipole order L and frequency ω from state i to state f, and I_i and I_f are the spins of the initial and final states (1)(40). From the gamma-ray relative intensities (Table 1), the following branching ratios of reduced transition probabilities were computed using equation 3.

$B(63.12\ \text{kev}) : B(240.4) : B(261.0) = 3.2 \times 10^3 : 1 : 6$

$B(177.24\ \text{kev}) : B(197.97) : B(307.7) = 2.5 \times 10^4 : 3 \times 10^4 : 1$

$B(109.78\ \text{kev}) : B(118.20) = 4.5 \times 10^3 : 1$

The branching ratios for the 63.12, 240.4, and the 261.0 kev transitions indicate that the 240.4 and the 261.0 kev gamma-rays are strongly suppressed compared to the 63.12 kev gamma-ray. Since all three of these transitions are most likely E1, suppression of the 240.4 and the 261.0 kev lines can be explained as being due to K forbiddeness. The fact that these transitions occur indicates that K is not a rigid quantum number and that the initial and final levels are mixed with states having differing K numbers.

The theoretical branching ratios of the reduced transition probabilities for gamma-radiation of multipole order L from an initial state with spin I_i to different members of a rotational band having spins I_f and I_f' is given by

$$\frac{B(L,\ I_i \rightarrow I_f)}{B(L,\ I_i \rightarrow I_{f'})} = \frac{\langle I_i\ L\ K_i\ K_f\text{-}K_i \mid I_i\ L\ I_f\ K_f\rangle^2}{\langle I_i\ L\ K_i\ K_f\text{-}K_i \mid I_i\ L\ I_{f'}\ K_f\rangle^2} \qquad (4)$$

where K_i and K_f denote the K quantum numbers of the initial and final states respectively (40). The bracketed terms on the right are Clebsch-Gordon coefficients. Using equation 4 and evaluating the Clebsch-Gordon coefficients (41), the theoretical branching ratio for E2 radiation from level C.

(fig. 7) to levels B. and A. can be computed to be

$$\frac{B(2,\ 5/2 \rightarrow 3/2)}{B(2,\ 5/2 \rightarrow 1/2)} = \frac{\langle 5/2\ 2\ 1/2\ 0 \mid 5/2\ 2\ 3/2\ 1/2\rangle^2}{\langle 5/2\ 2\ 1/2\ 0 \mid 5/2\ 2\ 1/2\ 1/2\rangle^2} = 2/7$$

From this value and from the 109.78 and 118.20 kev measured gamma-ray intensities (Table 1), the 109.78 kev transition is predicted to be 98% M1 + 2% E2, in agreement with the conversion coefficients given in Table 4. Similarly, from the measured gamma-ray intensities of the 177.24, 197.97 and 307.7 kev transitions, the 177.24 and 197.97 kev transitions are found also to be predominately M1, in agreement with the observed conversion coefficients in Table 4.

Alaga (42) has studied the limiting case of very large nuclear deformations and has given the set of quantum numbers ($N, \mu_z, \Lambda, \Omega$) for the classification of states. N is the principal quantum number of the oscillator, μ_z the quantum number for oscillations along the asymmetry axis, Λ the component of the particle orbital angular momentum along the symmetry axis, and Ω (= K) the component of the total particle angular momentum along the symmetry axis. Alaga has also given selection rules for beta transitions.

Tables 9 and 10 (Appendix III) give the $N, \mu_z, \Lambda, \Omega$ quantum numbers for the odd-proton and odd-neutron states listed by Mottelson and Nilsson. The selection rules given by Alaga (42) for allowed and first-forbidden beta transi-

tions are listed in Table 11 (Appendix III).

According to the (N, μ_z, Λ, Ω) description of states, levels A., B., C., and D. are described by (4, 1, 1, 1/2), level E. by (4, 0, 4, 7/2) and levels F. and G. by (5, 2, 3, 7/2). The ($i_{13/2}$, 7/2) groundstate (Table 8, Appendix III) of Yb^{169} would be given by (6, 3, 3, 7/2).

Beta transitions which obey the selection rules for I and Ω but which violate the selection rules for N, μ_z or Λ are designated by Alaga as hindered, while transitions which obey all selection rules are classed as unhindered. According to these selection rules, the electron-capture transitions from the (6, 3, 3, 7/2) Yb^{169} groundstate to Tm^{169} levels G. and F., which have (5, 2, 3, 7/2), are first-forbidden and unhindered with $\Delta N = -1$, $\Delta\mu_z = -1$, $\Delta\Lambda = 0$, $\Delta\Omega = 0$, yes. An allowed transition from the Yb^{169} groundstate to Tm^{169} level E. is hindered by $\Delta N = -2$, $\Delta\mu_z = -3$, and $\Delta\Lambda = 1$. The observed decay fractions (Table 4) indicate the electron capture to level E. to be not more than 10% of the total decay. Similarly, allowed transitions from the Yb^{169} groundstate to the K = 1/2 rotational band, which has (4, 1, 1, 1/2), besides being K forbidden, are hindered by having $\Delta N = -2$, $\Delta\mu_z = -2$ and $\Delta\Lambda = -2$. An upper limit for the electron capture to the K = 1/2 band can be given as 10% of the total decay.

The gamma-ray selection rules (Table 11, Appendix III)

may explain the lack of an observed crossover transition between levels G. and E. since for this transition $\Delta\mu_z = -2$. Similarly, the 63.12 kev transition is hindered by $\Delta\mu_z = -2$ which may explain the successful competition of the K-forbidden 240.4 and 261.0 kev transitions with the 63.12 kev transition.

That level E. is a metastable state, as determined by Johansson (28), would be expected since M1 and E2 transitions from this level to the K = 1/2 band are K-forbidden. In addition M1 transitions to the K = 1/2 band from level E. are hindered by $\Delta\mu_z = 1$ and $\Delta\Lambda = -3$.

PART V

LEVELS IN Lu^{175}

LEVELS IN Lu^{175}

A SUMMARY OF RESULTS AND LEVEL SCHEME

The decay of $_{70}Yb^{175}_{105}$ by beta-emission to $_{71}Lu^{175}_{104}$ was first reported by Atterling and collaborators in 1945 (43). The half-life of the beta-decay is 102 hours (10). The spectrum from the nuclear de-excitation of Lu^{175} following the decay from Yb^{175} has been extensively investigated. Cork and collaborators (23)(24), Marty (44), H. de Waard (45), Akerlind, et al. (46), and J. P. Mize and coworkers (19), have published measurements of the Lu^{175} spectrum.

The results of the present investigation are summarized in Table 5 and Figure 8.

The energies listed for the transitions were obtained from curved-crystal spectrometer measurements.

Each conversion coefficient was obtained by taking the ratio of the conversion line intensity (Table 3) to the corresponding gamma-ray intensity (Table 1). Since in the Lu^{175} spectrum there was no pure multipole transition suitable for normalizing the experimental ratios to the theoretical conversion coefficient, the Tm^{169} 130.53 kev K-conversion coefficient was used for this purpose. Gamma-ray intensities of the Lu^{175} 137.65, 144.85 and the Tm^{169} 130.53 kev transitions were measured with the curved-crystal spectrometer, while simultaneously the relative intensities of the corre-

Table 5. Comparison of Experimental and Theoretical Conversion Coefficients

Lu^{175}

Initial and final levels	Energy kev	α_K Exp.	α_K Theoretical E1	E2	M1	M2	α_L Exp.	α_L Theo. E1	M2	α Total	I_γ	Decay fraction %	Multipole assignment
BA	113.81	1.6	0.21	0.73	2.2	15.5				2.6	310	50	M1+E2
CB	137.65	1.0	0.13	0.45	1.3	8.0				1.6	22	2.5	M1+E2
EC	144.85	0.11	0.11	0.40	1.1	6.6				0.12	59	2.9	E1
CA	251.3	-								0.13	40	2.0	(E2)
EB	282.57	0.030	0.020	0.063	0.17	0.68	0.0037	0.0030	0.14	0.03	620	28	E1+M2
EA	396.1	0.067	0.0091	0.026	0.071	0.235	0.0085	0.0012	0.042	0.08	1000	48	E1+M2

		α_{L_I} Exp.	α_{L_I} Theo. M1	E2	$\alpha_{L_{II}}$ Exp.	$\alpha_{L_{II}}$ Theo. M1	E2	$\alpha_{L_{III}}$ Exp.	$\alpha_{L_{III}}$ Theo. M1	E2
BA	113.81	0.39	0.39	0.074	0.10	0.034	0.53	0.13	0.002	0.48

sponding K-conversion lines were measured with the ring-focusing beta-ray spectrometer. The ratios of the conversion line intensities to the gamma-ray intensities for the Lu^{175} transitions were then normalized to the theoretical E2 conversion coefficient for the K-line of the Tm^{169} 130.53 kev transition.

The theoretical K-shell conversion coefficients were interpolated from the tables by Sliv (31), while the theoretical L sub-shell coefficients were obtained from tables by Rose, et al. (30) and by Gellman, et al. (33), as in the case of Tm^{169} (Table 4).

According to the data in Table 5, the following approximate multipole admixture percentages are obtained:

Energy kev	Admixtures
113.81	80% M1 + 20% E2
137.65	70% M1 + 30% E2
282.57	98% E1 + 2% M2
396.1	80% E1 + 20% M2

Within experimental errors, these results are in agreement with similar data obtained by Mize, et al. (19).

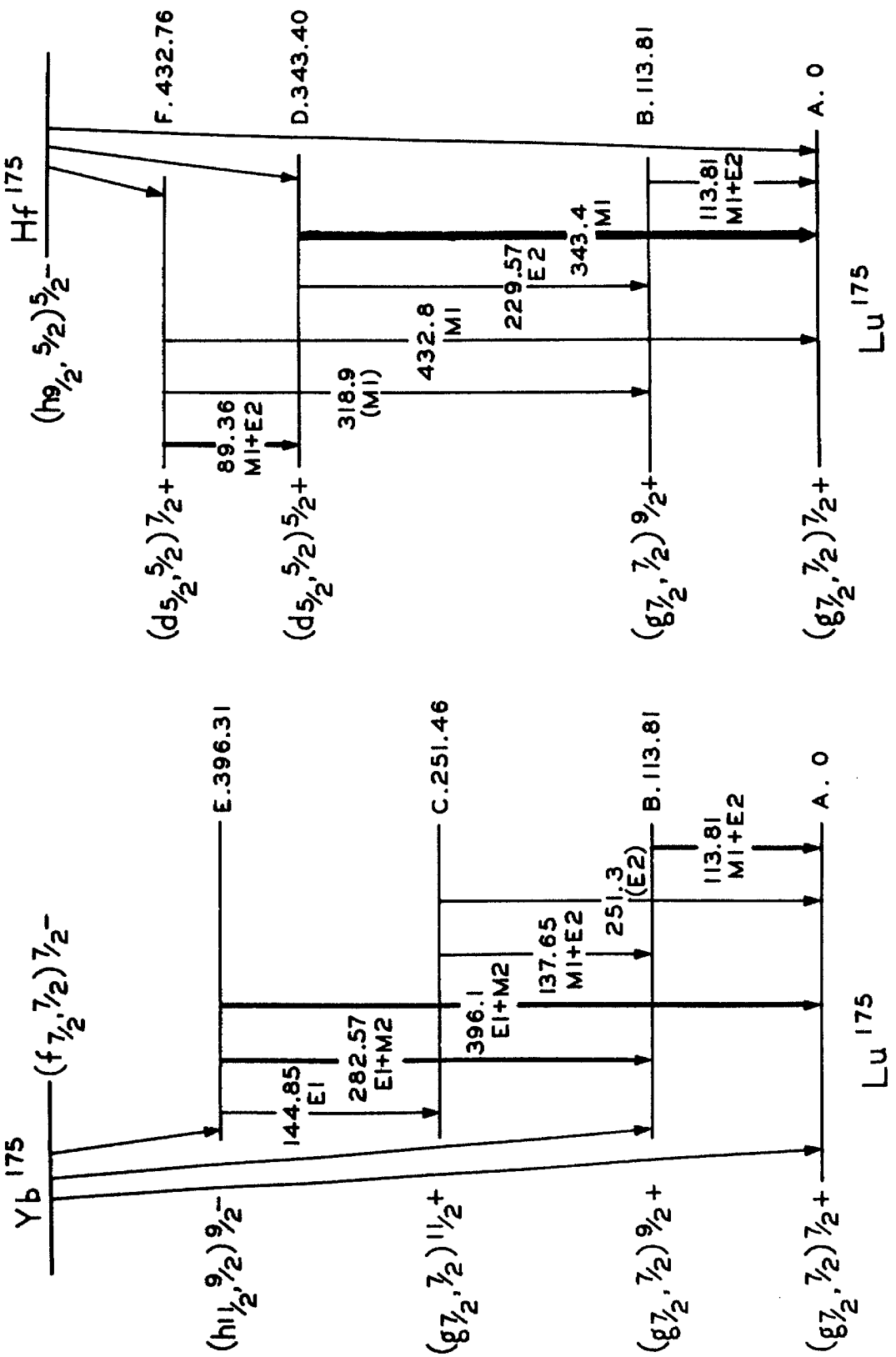

Figure 8. Lu^{175} level scheme.

The observed levels in Lu^{175} are shown in fig. 8. The notations and the procedure in establishing this level scheme are the same as in the case of Tm^{169} (fig. 7). The level scheme on the left represents the observed levels from measurements of transitions in Lu^{175} following beta-decay from Yb^{175}, while the level scheme on the right represents the levels in Lu^{175} observed from measurements of transitions following electron capture from Hf^{175} (47).

Mize, et al. (19) have determined that the high energy component of the Yb^{175} beta decay goes to the groundstate, level A. From the present measurements of the end-point energy of the decay to level A. and of the energies of levels B. and E., taking into account the decay fractions into and out of each level, the following energies and log ft values of the three components of the Yb^{175} beta decay were obtained:

	E_{max} kev	log ft
To level A.	465 ± 5	6.4
B.	351 ± 5	7.2
E.	69 ± 5	4.5

B DISCUSSION

The ($g_{7/2}$, K = 7/2) groundstate predicted from Nilsson's calculations of individual particle levels in deformed nuclei (3)(4) (see Table 7, Appendix III) is in agreement with the measured groundstate spin of 7/2 (48).

Measurements of gamma-rays following the Coulomb excitation of Lu^{175} have shown that the 113.81 and 250.5 kev gamma-rays arise from transitions from the first and second rotational states above the ($g_{7/2}$, K = 7/2) groundstate (34) (49).

Energy Spacing of the Rotational Levels

Lu^{175}, like Tm^{169}, lies in a region of large nuclear deformations, and according to the unified model (2), the Lu^{175} spectrum should exhibit rotational characteristics. That the 113.81 and 251.5 kev levels are rotational in character is evident from how closely the levels fit the predicted rotational spectrum, which according to the unified model is given by

$$E_{7/2}(I) = E_{7/2}^{(0)} + E_{7/2}^{(1)}\, I(I+1) + E_{7/2}^{(2)}\, I^2(I+1)^2 \qquad (5)$$

where $E^{(0)}$ is chosen to give the groundstate zero energy, and $E^{(1)}$ equals $h^2/2\mathcal{I}$, $\mathcal{I}$ being the moment of inertia of the nuclear deformation. The $E_{7/2}^{(2)} I^2\,(I+1)^2$ is a fairly small, usually negative, correction term.

If the $E_{7/2}^{(2)}\, I^2(I+1)^2$ term is neglected and $E_{7/2}^{(0)}$ and

$E^{(1)}_{7/2}$ are determined by fitting equation 5 to the measured energies of states A. and B., $E^{(0)}_{7/2}$ = -199.17 kev and $E^{(1)}_{7/2}$ = 12.646 kev are obtained. From these values level C. is predicted to have an energy $E_{7/2}(11/2)$ = 252.91 kev, which can be compared with the measured value of 251.46 kev. When the measured energies of $E_{7/2}(7/2)$ = 0 kev, $E_{7/2}(9/2)$ = 113.81 kev and $E_{7/2}(11/2)$ = 251.46 kev are fitted to equation 5, including the second-order correction term, we obtain

$$E^{(0)}_{7/2} = - 201.74 \text{ kev}$$

$$E^{(1)}_{7/2} = 12.913 \text{ kev}$$

$$E^{(2)}_{7/2} = - 0.006595 \text{ kev.}$$

From these values a level at $E_{7/2}(13/2)$ = 412.08 kev is predicted. No transitions to or from this level have been observed.

Interpretation of Levels

An analysis of the nuclear levels in Lu^{175} using the data obtained by Mize, Bunker and Starner (19) has been made by Chase and Wilets (50). Following the results of Nilsson's calculations of individual particle levels (3)(4) (see Table 7, Appendix III), Chase and Wilets interpret level E. to be the ($h_{11/2}$, K = 9/2) particle excitation.

Measurements of transitions from levels excited in Lu^{175} by electron capture from Hf^{175} have been carried out with neutron irradiated Hf sources which had been previously enriched in Hf^{174} (19)(47)(51). The transitions observed from the measurements in this laboratory (47) are shown in the level scheme on the right-hand side of fig. 8. The only transition common to both level schemes is the one at 113.81 kev. The levels D. and F. are interpreted as belonging to the rotational band based on the $(d_{5/2}, 5/2)$ single particle excitation (50) (Assuming the rotational splitting constant $E_{7/2}^{(1)} = 12.913$ kev, obtained by fitting equation 5 to levels A., B., and C., neglecting the second order correction, the energy of the transition between levels F. and D. is predicted to be 90.39 kev, which compares closely with the measured value of 89.36 kev).

From Table 8, Appendix III, the groundstate of Yb^{175} is designated by $(f_{7/2}, 7/2)$ and the Hf^{175} groundstate by $(h_{9/2}, 5/2)$.

Transition Intensities

According to the $(N, \mu_z, \Lambda, \Omega)$ (42) description for states, from Tables 9 and 10, Appendix III, the Lu^{175} states A., B., and C. are described by (4, 0, 4, 7/2), states D. and F. by (4, 0, 2, 5/2), and level E. by (5, 1, 4, 9/2). The groundstate of Yb^{175} should correspond to (5, 1, 4, 7/2), while the groundstate of Hf^{175} should be described by (5, 1, 2, 5/2).

The first-forbidden beta-decay transitions from the Yb^{175} groundstate to levels A. and B. (log ft = 6.4 and 7.2, respectively) are unhindered by Alaga's selection rules (Table 11, Appendix III) with $\Delta N = -1$, $\Delta \mu_2 = -1$, $\Delta \Lambda = 0$, $\Delta \Omega = 0$, yes (42). The allowed beta decay from Yb^{175} to level E. (log ft = 4.5) is also unhindered by the selection rules with $\Delta N = 0$, $\Delta \mu_2 = 0$, $\Delta \Lambda = 0$, $\Delta \Omega = 1$, no. Yb^{175} first-forbidden decay to Lu^{175} levels D. and F. was not observed. Observation of this decay would not seem likely since it would be in competition with the allowed decay to level E. and the more energetic first-forbidden decay to A. and B. In addition this decay would be hindered by $\Delta \Lambda = -2$. Similarly, no electron capture from Hf^{175} to Lu^{175} level E. was observed, and the transition would be unlikely because of spin change $\Delta I = 2$.

The observed electron capture from Hf^{175} to Lu^{175} levels D. and F. has been discussed by Alaga (42). The fact that electron capture from Hf^{175} to levels D. and F. competes successfully with the more energetic transition to the Lu^{175} groundstate is attributed to the latter transition being hindered by $\Delta \Lambda = 2$.

No gamma-ray transitions between levels F. and E., E. and D., or D. and C. have been observed. The E1 transition rate between F. and E. should be reduced because of K-forbiddeness, and M2 transitions between F. and E. would not be likely in

competition with the 89.36 M1 + E2 transition to level D. An M2 transition between levels E. and D. would not be likely in competition with lower multipole transitions to the K = 7/2 band. An E2 transition from level F. to level C. would be expected to be below the level of observation in competition with the more energetic, but comparatively weak (47) 318.9 kev (M1) transition. The fact that the 318.9 and 432.8 kev transitions are less intense than the 89.36 kev transition (47) may be due to the former two transitions being hindered by $\Delta\Lambda = 2$ (see Table 11, Appendix III), while the latter transition is unhindered.

The theoretical branching ratio of the reduced transition probabilities for gamma-radiation from some initial state to two different members of a rotational band was given by equation 4 (Part IV). If it is assumed that the 144.85, 282.57, and 396.1 kev transitions are principally E1, the theoretical and experimental branching ratios can be compared. The experimental ratios can be obtained from the gamma-ray intensities (Table 1) using equation 3 (Part IV), while the theoretical ratios can be computed with equation 4. The experimental branching ratios for the 144.85, 282.57, and 396.1 kev gamma-rays obtained using equation 3 are:

$$B(144.85 \text{ kev}) : B(282.57) : B(396.1) = 7 : 10 : 6$$

The corresponding theoretical ratios are:

$$B(1,\ 9/2 \rightarrow 11/2) : B(1,\ 9/2 \rightarrow 9/2) : B(1,\ 9/2 \rightarrow 7/2) =$$

$$1 : 10 : 44$$

The discrepancy between the theory and experiment may be due to mixing of states from different rotational bands.

Conclusion

The results of the present investigations have verified several features of the unified model of the nucleus. In the case of both Tm^{169} and Lu^{175}, the energy spacings in rotational bands according to this model agree with the precision measurements to within one per cent. In addition, the spin and parity assignments to the low lying intrinsic excitations appear to be in good agreement with the calculations of individual particle levels.

It will be of interest to extend such investigations to other deformed nuclei and to search for additional regularities in the patterns of their excited states.

APPENDICES

APPENDIX I

Curved-crystal Spectrometer and Beta-ray Spectrometer Sources

Of the seven stable isotopes of ytterbium, only Yb^{168}, Yb^{174}, and Yb^{176} form radioactive isotopes following neutron capture. Some of the properties of these three isotopes are listed below.

Isotope	Isotopic abundance (10) %	Neutron capt. cross sect.(52) barns	Radioactive isotope	Mode of decay and half-life(10)	Daughter
Yb^{168}	0.140	11,000+3,000	Yb^{169}	e-capt. 31.8	Tm^{169}
Yb^{174}	31.84	60±40	Yb^{175}	β^- 102 h	Lu^{175}
Yb^{176}	12.73	7±2	Yb^{177}	β^- 1.8 h	Lu^{177}

The radioactive ytterbium sources were prepared from Yb_2O_3 powder purchased from Research Chemicals, Inc., Burbank, California (Lot #452). The manufacturer stated the purity of the Yb_2O_3 to be 99.8% with contaminations $< 0.1\%$ Tm, and traces of Eu and Sm. There were no observable traces of Lu.

Yb_2O_3 powder was neutron irradiated in the Phillips Petroleum Company Materials Testing Reactor at Arco, Idaho on two separate occasions. During the first irradiation, which took place in April 1955, 10 mgs of Yb_2O_3 was irradiated for 11 days at an average neutron flux of 1.5×10^{14} neutrons/cm^2/sec. The second irradiation was secured in

order to obtain a stronger curved-crystal spectrometer source to search for weak gamma-lines in the Tm^{169} spectrum. In November 1955, 50 mgs of Yb_2O_3 was irradiated for 19 days at an average neutron flux of 5×10^{13} neutrons/cm^2/sec. The curved-crystal spectrometer source from the 50 mgs of Yb_2O_3 had an intensity of approximately one curie when placed in the spectrometer.

Curved-crystal Spectrometer Sources

Two types of Yb sources were employed for the curved-crystal spectrometer measurements. One type, which was used for the relative intensity and precision energy measurements, consisted of a small quartz capillary tube having an outside diameter of about 0.100" and a capillary diameter of 0.008", filled with 6 mgs of Yb_2O_3 to a depth of 2 cm. The tube was sealed off at the bottom and had a small conical funnel ground into the top to facilitate filling. After the capillary was filled and the top sealed off, it was ready for irradiation. The quartz capillary being a line source of gamma-rays, was placed in a lucite holder which positioned the capillary by means of a V-shaped groove machined in one surface (fig. 9).

The second type of curved-crystal spectrometer Yb source was obtained by depositing 50 mgs of radioactive Yb_2O_3 into a depression 1 cm x 2 cm x 0.080", machined into a lucite holder. The Yb was sealed inside the depression by

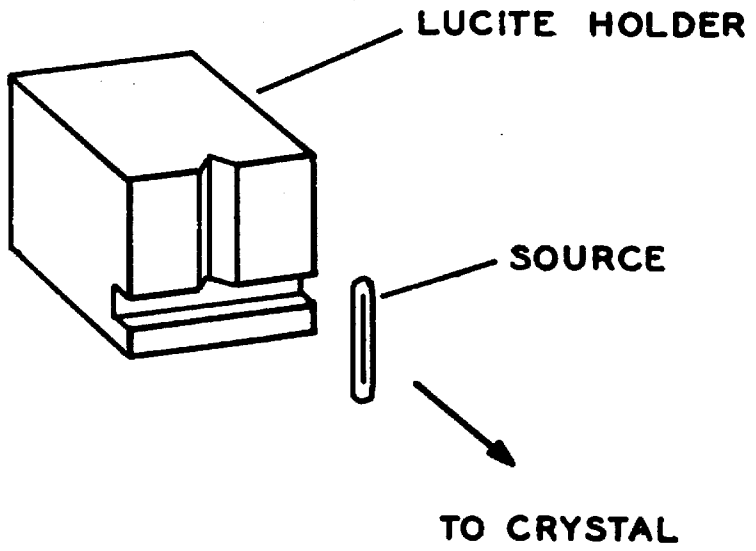

ASSEMBLY FOR SOURCE SEALED IN QUARTZ CAPILLARY.

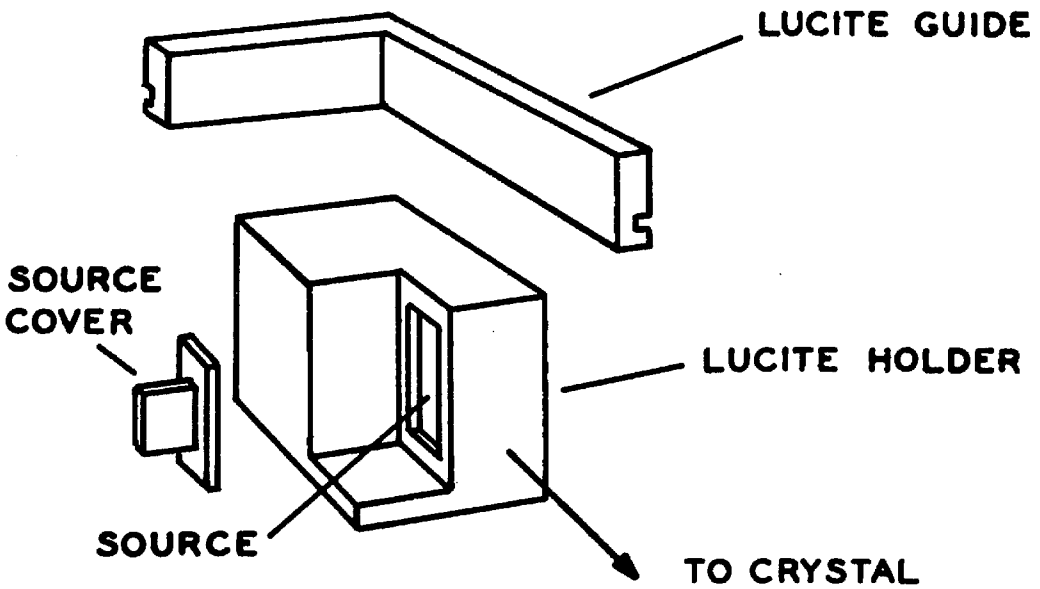

ASSEMBLY FOR 50 MG. Yb SOURCE.

Figure 9. Source assembly for curved-crystal spectrometer.

by a lucite cap. The effective width of this source on the spectrometer focal circle was 0.020". The lucite source holder was positioned in the spectrometer with a lucite guide and was held in place with rubber bands (fig. 9).

Beta-ray Spectrometer Sources

Internal conversion sources for the ring-focusing spectrometer were provided by evaporating radioactive Yb_2O_3 upon a thin sheet of mica and subsequently punching small discs from the mica. To obtain 0.35% momentum resolution, discs 1.5 mm in diameter were employed.

The internal conversion source for the semicircular spectrometer consisted of a strip of mica .12 cm x 4 cm with an invisible layer of radioactive Yb_2O_3 evaporated on it.

In the case of the disc sources, a very thin coating of aluminum was evaporated over the source to avoid an electrical charging effect. The strip sources were grounded using Aquadag.

The gamma-ray source for measuring the relative intensities of Tm^{169} gamma-rays by means of the photoelectric effect in an external converter, was 3 mgs of radioactive Yb_2O_3 inserted into a beta-ray absorbing copper capsule. The photo effect took place in the lead or uranium converter on the aluminum cover which was inserted over the source containing capsule.

Figure 10 shows the energy dependence of the photo-electric absorption coefficients of uranium L-shells computed from formulas derived by Hall and by Stobbe (18).

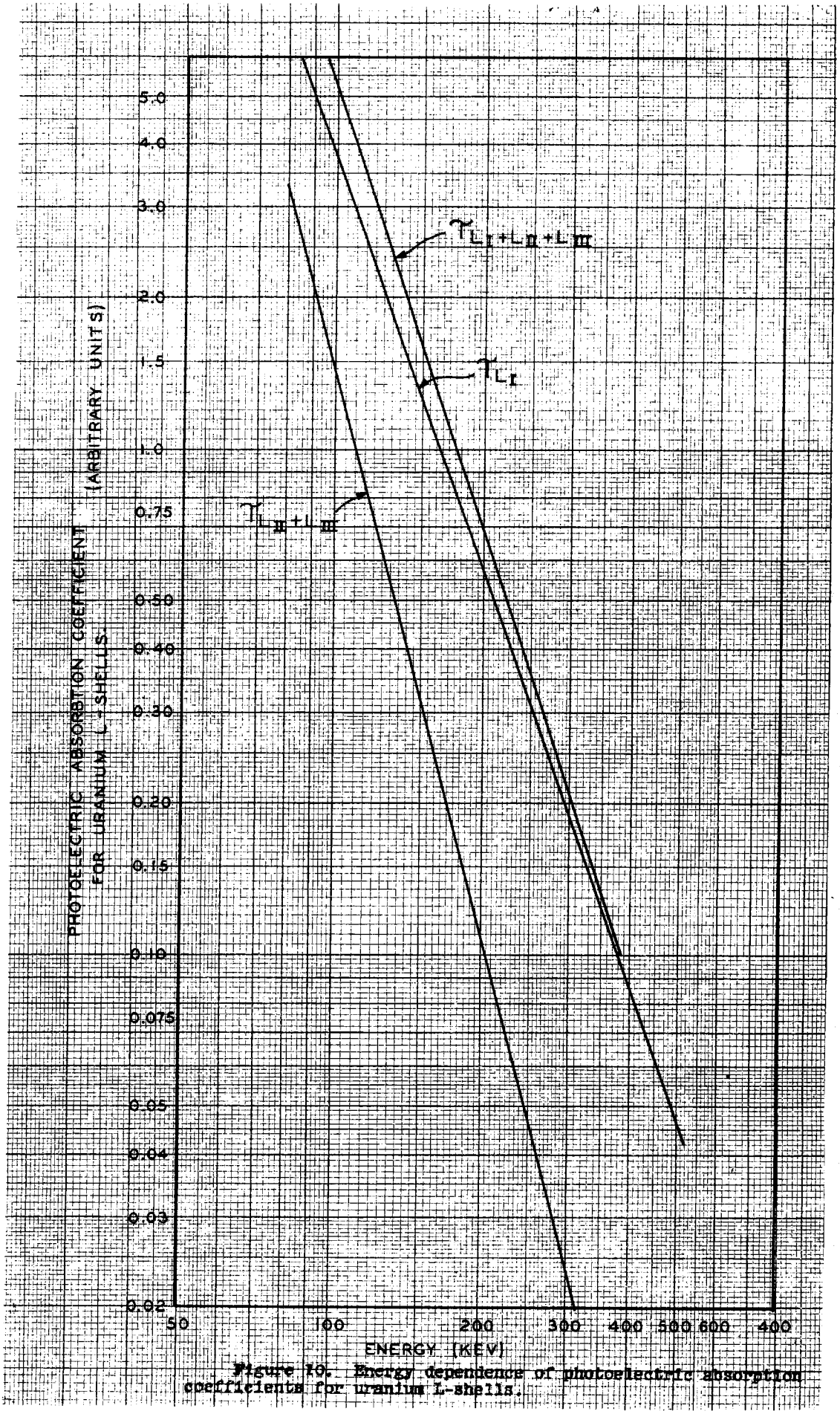

Figure 10. Energy dependence of photoelectric absorption coefficients for uranium L-shells.

APPENDIX II

ADDITIONAL CURVED-CRYSTAL SPECTROMETER MEASUREMENTS

Table 6 lists curved-crystal spectrometer measurements of $K\alpha_1$ and $K\alpha_2$ x-rays from Tm, Yb, Lu , Hf, and Ta. Tm $K\alpha$, Yb $K\alpha$, and Lu $K\alpha$ x-rays were emitted by the Yb source, while the Lu $K\alpha$, Hf $K\alpha$, and the Ta $K\alpha$ x-rays were emitted from a neutron irradiated Hf source. The energy of the Yb^{170} gamma-ray emitted from a neutron irradiated Tm sample is also listed.

The well known Ta $K\alpha_1$ line from the Hf source was the standard for all measurements.

Table 6. Curved-crystal Spectrometer Measurements

	λ(x.u.)	E(kev)	
$_{69}Tm\ K\alpha_2$	248.60 ± 0.02	49.77 ± 0.01	
$_{69}Tm\ K\alpha_1$	243.86 ± 0.02	50.74 ± 0.01	
$_{70}Yb\ K\alpha_2$	240.94 ± 0.02	51.35 ± 0.01	
$_{70}Yb\ K\alpha_1$	236.19 ± 0.02	52.38 ± 0.01	
$_{71}Lu\ K\alpha_2$	233.61 ± 0.02	52.96 ± 0.01	
$_{71}Lu\ K\alpha_1$	228.83 ± 0.02	54.07 ± 0.01	
$_{72}Hf\ K\alpha_2$	226.61 ± 0.02	54.60 ± 0.01	
$_{72}Hf\ K\alpha_1$	221.81 ± 0.02	55.78 ± 0.01	
$_{73}Ta\ K\alpha_2$	219.85 ± 0.02	56.28 ± 0.01	
$_{73}Ta\ K\alpha_1$	215.050± 0.015	57.53 ± 0.01	standard
	Yb^{170} Gamma-ray		
	146.84 ± 0.03	84.26 ± 0.02	

APPENDIX III

TABLES 7-11

Tables 7 and 8 represent the order of individual particle levels between closed shells given by Mottelson and Nilsson (4) for odd proton and odd neutron nuclei corresponding to deformation parameter $\delta = 0.28$.

Each level is labeled on the left with its corresponding single particle orbit for a spherical nucleus (e.g., $g_{7/2}$), which represents the limiting state as the deformation tends to zero, and with its spin and parity; and on the right with the orbit number used by Nilsson.

For Table 7 the Z = 49 shown on the lower right of the table indicates that orbit 30 contains the last odd proton when Z = 49. Similarly, orbit 28 contains the last odd proton when Z = 81. The same interpretation applies to N = 81 and N = 125 for odd neutron nuclei in Table 8.

These tables are, of course, diagrammatic, and no energy scale is attached to the level spacings. However, the levels which are shown as more closely spaced are those for which the ordering may be fortuitous.

Tables 9 and 10 give the N, μ_z, Λ and Ω quantum numbers (42) corresponding to the individual particle levels listed in tables 7 and 8 respectively. The author wishes to thank Dr. S. A. Moszkowski for providing tables 9 and 10.

Table 7. States Listed by Mottelson and Nilsson for Z odd, $\delta = 0.28$, in Order of Increasing Energy

$h_{11/2}$, 11/2, -	———	28 Z = 81
$s_{1/2}$, 1/2, +	———	51
$d_{3/2}$, 3/2, +	———	42
$h_{11/2}$, 9/2, -	———	32
$d_{5/2}$, 5/2, +	———	31
$g_{7/2}$, 7/2, +	———	25
$d_{3/2}$, 1/2, +	———	43
$h_{11/2}$, 7/2, -	———	35
$d_{5/2}$, 3/2, +	———	33
$g_{7/2}$, 5/2, +	———	27
$h_{11/2}$, 5/2, -	———	36
$h_{11/2}$, 3/2, -	———	37
$g_{9/2}$, 9/2, +	———	18
$g_{7/2}$, 3/2, +	———	29
$d_{5/2}$, 1/2, +	———	34
$h_{11/2}$, 1/2, -	———	38
$g_{7/2}$, 1/2, +	———	30 Z = 49

Table 8. States Listed by Mottelson and Nilsson for N odd, $\delta = 0.28$, in Order of Increasing Energy

$p_{1/2}$, 1/2, -		A N = 125
$f_{5/2}$, 5/2 -		61
$f_{5/2}$, 3/2 -		70
$i_{13/2}$, 13/2 +		39
$h_{9/2}$, 9/2 -		40
$i_{13/2}$, 11/2 +		45
$h_{9/2}$, 7/2 -		48
$p_{3/2}$, 3/2 -		62
$f_{5/2}$, 1/2 -		71
$i_{13/2}$, 9/2 +		49
$f_{7/2}$, 7/2 -		41
$h_{9/2}$, 5/2 -		50
$i_{13/2}$, 7/2 +		54
$p_{3/2}$, 1/2 -		63
$h_{11/2}$, 11/2 -		28
$f_{7/2}$, 5/2 -		44
$h_{9/2}$, 3/2 -		52
$i_{13/2}$, 5/2 +		55
$i_{13/2}$, 3/2 +		57
$f_{7/2}$, 3/2 -		46
$i_{13/2}$, 1/2 +		60
$h_{9/2}$, 1/2 -		53
$f_{7/2}$, 1/2 -		47 N = 81

Table 9. N, μ_z, Λ, and Ω for States Listed in Table 7

Z odd	Orbit No.	Ω	π	Sph. limit	N	μ_z	Λ
49	30	1/2	+	$g_{7/2}$	4	3	1
51	38	1/2	-	$h_{11/2}$	5	5	0
53	34	1/2	+	$d_{5/2}$	4	2	0
55	29	3/2	+	$g_{7/2}$	4	2	2
57	18	9/2	+	$g_{9/2}$	4	0	4
59	37	3/2	-	$h_{11/2}$	5	4	1
61	36	5/2	-	$h_{11/2}$	5	3	2
63	27	5/2	+	$g_{7/2}$	4	1	3
65	33	3/2	+	$d_{5/2}$	4	1	1
67	35	7/2	-	$h_{11/2}$	5	2	3
69	43	1/2	+	$d_{3/2}$	4	1	1
71	25	7/2	+	$g_{7/2}$	4	0	4
73	31	5/2	+	$d_{5/2}$	4	0	2
75	32	9/2	-	$h_{11/2}$	5	1	4
77	42	3/2	+	$d_{3/2}$	4	0	2
79	51	1/2	+	$s_{1/2}$	4	0	0
81	28	11/2	-	$h_{11/2}$	5	0	5

Table 10. N, μ_z, Λ, and Ω for States Listed in Table 8

N′ odd*	Orbit No.	Ω	π	Sph. limit	N	μ_z	Λ
81	47	1/2	-	$f_{7/2}$	5	4	1
83	53	1/2	-	$h_{9/2}$	5	3	0
85	60	1/2	+	$i_{13/2}$	6	6	0
87	46	3/2	-	$f_{7/2}$	5	3	2
89	57	3/2	+	$i_{13/2}$	6	5	1
91	55	5/2	+	$i_{13/2}$	6	4	2
93	52	3/2	-	$h_{9/2}$	5	2	1
95	44	5/2	-	$f_{7/2}$	5	2	3
97	28	11/2	-	$h_{11/2}$	5	0	5
99	63	1/2	-	$p_{3/2}$	5	2	1
101	54	7/2	+	$i_{13/2}$	6	3	3
103	50	5/2	-	$h_{9/2}$	5	1	2
105	41	7/2	-	$f_{7/2}$	5	1	4
107	49	9/2	+	$i_{13/2}$	6	2	4
109	71	1/2	-	$f_{5/2}$	5	1	0
111	62	3/2	-	$p_{3/2}$	5	1	2
113	48	7/2	-	$h_{9/2}$	5	0	3
115	45	11/2	+	$i_{13/2}$	6	1	5
117	40	9/2	-	$h_{9/2}$	5	0	5
119	39	13/2	+	$i_{13/2}$	6	0	6
121	70	3/2	-	$f_{5/2}$	5	0	1
123	61	5/2	-	$f_{5/2}$	5	0	3
125	A.	1/2	-	$p_{1/2}$	5	0	1

*N′ denotes number of neutrons.

Table 11. N, μ_z, Λ, Ω Selection Rules for Beta- and Gamma-ray Transitions

Operators	Selection rules				
Selection rules for allowed beta-decay transitions					
1	$\Delta N=0$,	$\Delta\mu_z=0$,	$\Delta\Lambda=0$,	$\Delta\Omega=0$,	No
σ	$\Delta N=0$,	$\Delta\mu_z=0$,	$\Delta\Lambda=0$,	$\Delta\Omega=0,\pm1$	No
Selection rules for first forbidden beta-decay transitions					
$\sigma\cdot r$ $\sigma\cdot\nabla$	$\Delta N=\pm1$	$\Delta\mu_z=\pm1$ $\Delta\mu_z=0$,	$\Delta\Lambda=0$ $\Delta\Lambda=\pm1$	$\Delta\Omega=0$	Yes
r	$\Delta N=\pm1$	$\Delta\mu_z=\pm1$, $\Delta\mu_z=0$,	$\Delta\Lambda=0$, $\Delta\Lambda=\pm1$	$\Delta\Omega=0$ $\Delta\Omega=\pm1$	Yes
$\sigma\times r$ $\sigma\times\nabla$	$\Delta N=\pm1$	$\Delta\mu_z=\pm1$, $\Delta\mu_z=0$,	$\Delta\Lambda=0$, $\Delta\Lambda=\pm1$,	$\Delta\Omega=\pm1$ $\Delta\Omega=0,\pm1$	Yes
B_{ij}	$\Delta N=\pm1$	$\Delta\mu_z=\pm1$, $\Delta\mu_z=0$,	$\Delta\Lambda=0$, $\Delta\Lambda=\pm1$,	$\Delta\Omega=0,\pm1$ $\Delta\Omega=0,\pm1,\pm2$	Yes
Selection rules for E1 and M1 gamma-ray transitions					
E1	$\Delta N=\pm1$	$\Delta\mu_z=\pm1$ $\Delta\mu_z=0$,	$\Delta\Lambda=0$ $\Delta\Lambda=\pm1$	$\Delta\Omega=0$ $\Delta\Omega=\pm1$	Yes
M1	$\Delta N=0$,	$\Delta\mu_z=0$,	$\Delta\Lambda=0$,	$\Delta\Omega=0,\pm1$	No

The selection rules for the beta-ray transitions were given by Alaga (42). The E1 and M1 gamma-ray selection rules are the same as for the r and σ operators for beta decay respectively.

REFERENCES

1. A. Bohr and B. R. Mottelson, Kgl. Danske Videnskab. Selskab, Mat.-fys. Medd. 27, No. 16 (1953).

2. A. Bohr and B. R. Mottelson, Chapter 17, Beta- and Gamma-Ray Spectroscopy, edited by K. Siegbahn, North-Holland Publishing Company, Amsterdam, 1955.

3. S. G. Nilsson, Kgl. Danske Videnskab. Selskab, Mat.-fys. Medd. 29, No. 16 (1955).

4. B. R. Mottelson and S. G. Nilsson, Phys. Rev. 99, 1615 (1955).

5. D. E. Muller, H. C. Hoyt, D. J. Klein, and J. W. M. DuMond, Phys. Rev. 88, 775 (1952).

6. J. W. M. DuMond, Chapter 4, Beta- and Gamma-Ray Spectroscopy, edited by K. Siegbahn, North-Holland Publishing Company, Amsterdam, 1955.

7. J. W. M. DuMond, Rev. Sci. Inst. 20, 160 (1949).

8. J. W. M. DuMond, J. Kohl, L. Bogart, D. E. Muller, and J. R. Wilts, ONR Special Technical Report No. 16 (March, 1952).

9. Description of the semicircular spectrometer is in preparation.

10. J. M. Hollander, I. Perlman, and G. T. Seaborg, Rev. Mod. Phys. 25, 469 (1953).

11. P. Marmier and F. Boehm, Phys. Rev. 97, 103 (1955).

12. E. Ingelstam, Nova Acta Reg. Soc. Sci. upsal. 4, No. 5 (1936).

13. J. J. Murray, Jr., Ph.D. thesis, California Institute of Technology (1954).

14. D. Maeder, R. Müller and V. Wintersteiger, Helv. Phys. Acta 27, 3 (1954).

15. D. A. Lind, Ph.D. thesis, California Institute of Technology (1948).

16. D. A. Lind, W. J. West, and J. W. M. DuMond, Phys. Rev. 77, 475 (1950).

17. M. Stobbe, Ann. d. Phys. 7, 661 (1930).

18. C. M. Davisson, Chapter 2, Beta- and Gamma-Ray Spectroscopy, edited by K. Siegbahn, North-Holland Publishing Company, Amsterdam, 1955, p. 28.

19. J. P. Mize, M. E. Bunker, and J. W. Starner, Phys. Rev. 100, 1390 (1955).

20. S. A. Moszkowski, Phys. Rev. 82, 35 (1951).

21. W. Bothe, Z. Naturforschg. 1, 173 (1946).

22. D. S. Martin, Jr., E. N. Jensen, F. J. Hughes and R. T. Nichols, Phys. Rev. 82, 579 (1951).

23. J. M. Cork, H. B. Keller, W. C. Rutledge, and A. E. Stoddard, Phys. Rev. 78, 95 (1950).

24. J. M. Cork, M. K. Brice, D. W. Martin, L. C. Schmid, and R. G. Helmer, Phys. Rev. 101, 1042 (1956).

25. S. DeBenedetti and F. K. McGowan, Phys. Rev. 74, 728 (1948).

26. E. W. Fuller, Proc. Phys. Soc. London 63A, 1044 (1950).

27. A. W. Sunyar and J. W. Mihelich, Phys. Rev. 81, 300 (1951).

28. S. A. E. Johansson, Phys. Rev. 100, 835 (1955).

29. T. Huus, J. H. Bjerregaard, and B. Elbek, Kgl. Danske Videnskab. Selskab, Mat.-fys. Medd. 30, No. 17 (1956).

30. M. E. Rose, G. H. Goertzel, and C. Swift (privately circulated tables).

31. L. Sliv (privately circulated tables).

32. A. H. Wapstra and G. J. Nijgh, Nuclear Physics 1, No. 4, 245 (1956).

33. H. Gellman, B. A. Griffith, and J. P. Stanley, Phys. Rev. 85, 944 (1952).

34. N. P. Heydenburg and G. M. Temmer, Phys. Rev. 100, 150 (1955).

35. K. Way and M. Wood, Phys. Rev. 94, 119 (1953).

36. H. Schüler and T. Schmidt, Naturwiss. 22, 838 (1934).

37. K. H. Lindenberger and A. Steudel, Naturwiss. 42, 41 (1955).

38. B. R. Mottelson and S. G. Nilsson, Z. Physik 141, 217 (1955).

39. A. K. Kerman, Kgl. Danske Videnskab. Selskab, Mat.-fys. Medd. 30, No. 15 (1956).

40. G. Alaga, K. Alder, A. Bohr, and B. R. Mottelson, Kgl. Danske Videnskab. Selskab, Mat.-fys. Medd. 29, No. 9 (1955).

41. E. U. Condon and G. H. Shortley, The Theory of Atomic Spectra, Cambridge University Press (1953), pp. 76-77.

42. G. Alaga, Phys. Rev. 100, 432 (1955).

43. H. Atterling, E. Bohr, and T. Sigurgeirsson, Arkiv Mat., Astron. Fysik 32A, No. 2 (1945).

44. N. Marty, Compt. rend. 240, 963 (1955).

45. H. de Waard, Phil. Mag. 46, 445 (1955).

46. L. Akerlind, B. Hartmann, and T. Wiedling, Phil. Mag. 46, 448 (1955).

47. F. Boehm, E. N. Hatch, P. Marmier, and J. W. M. DuMond (To be published).

48. H. Schüler and T. Schmidt, Z. Physik 95, 265 (1935).

49. C. McClelland, H. Mark, and C. Goodman, Phys. Rev. 97, 1191 (1955).

50. D. M. Chase and L. Wilets, Phys. Rev. 101, 1038 (1956).

51. A. O. Burford, J. F. Perkins, and S. K. Haynes, Phys. Rev. 99, 3 (1955).

52. Handbook of Chemistry and Physics (36th Edition), Chemical Rubber Publishing Co., Cleveland, 1954, pp. 448-454.